From DEPARTMENT OF CLINICAL NEUROSCIENCE
Karolinska Institutet, Stockholm, Sweden

DEVELOPMENT OF NOVEL 5-HT$_{1B}$ PET RADIOLIGANDS

Anton Lindberg

Karolinska Institutet

Stockholm 2019

Cover Illustration:

Transaxial PET summation images (0-123 min) using [^{18}F]AZ10419096 in baseline PET measurement (left) and PET measurement after pretreatment with AR-A000002 (2.0 mg/kg) given 30 min before radioligand (right).

All previously published papers were reproduced with permission from the publisher.
Published by Karolinska Institutet.
Printed by US-AB, Stockholm, Sweden
© Anton Lindberg, 2019
ISBN 978-91-7831-489-8

Development of novel 5-HT_{1B} PET radioligands

THESIS FOR DOCTORAL DEGREE (Ph.D.)

By

Anton Lindberg

Principal Supervisor:
Professor Christer Halldin
Karolinska Institutet
Department of Clinical Neuroscience

Co-supervisor(s):
Dr. Victor W. Pike
National Institute of Mental Health
Molecular Imaging Branch
Bethesda, MD, USA

Dr. Magnus Schou
AstraZeneca PET Science Centre
Karolinska Institutet
Department of Clinical Neuroscience

Dr. Sangram Nag
Karolinska Institutet
Department of Clinical Neuroscience

Dr. Charles S. Elmore
AstraZeneca Early Chemical Development
Isotope Chemistry

Opponent:
Dr. Jan Passchier
Invicro LLC
Senior vice President
Global Head of Chemistry
London, UK

Examination Board:
Professor Jan Bergman
Karolinska Institutet
Department of Bioscience and Nutrition

Professor Dirk Bender
Aarhus University Hospital
Department of Nuclear Medicine and PET Centre
Aarhus, Denmark

Dr. Thuy Tran
Karolinska Institutet
Department of Clinical Neuroscience
Stockholm, Sweden

ABSTRACT

Positron emission tomography (PET) is a useful tool for studying the central nervous system (CNS) in living subjects. PET is a non-invasive imaging technique that can visualize biochemical process such as receptor-ligand interactions and has been utilized for several neurotransmitter systems including the serotoninergic system. Serotonin receptor subtype 1B (5-HT_{1B}) is an interesting target to study using PET and two radioligands have been developed for this purpose, [^{11}C]AZ10419369 and [^{11}C]P943. Both are labelled with carbon-11 and have been used in various PET studies during the last decade. One type of PET study that [^{11}C]AZ10419369 and [^{11}C]P943 have been used for is measuring changes in endogenous 5-HT concentrations in brain. *In vitro* models show that an agonist could be more sensitive to competition from endogenous 5-HT than an antagonist. [^{11}C]AZ10419369 and [^{11}C]P943 were both originally presented as antagonists, but [^{11}C]AZ10419369, at least, has been shown to have agonist efficacy. Both [^{11}C]AZ10419369 and [^{11}C]P943 are also labelled with shorter-lived radionuclide carbon-11 ($t_{1/2}$ = 20.4 min) which limits their use to facilities with a cyclotron. A fluorine-18 ($t_{1/2}$ = 109.7 min) would allow more facilities to conduct PET studies on 5-HT_{1B}.

In this thesis the aim has been to develop a full antagonist and agonist 5-HT_{1B} PET radioligand in order to be able to assess whether their intrinsic activity affects their sensitivity towards changes in endogenous 5-HT concentrations. From a library of over 3000 compounds, provided by AstraZeneca, candidates were selected primarily with respects to their affinity, intrinsic activity and lipophilicity. *Paper I* describes the development of a full antagonist 5-HT_{1B} PET radioligand labelled with carbon-11, [^{11}C]AZ10419096, with high specific binding and sensitivity to displacement by endogenous 5-HT. *Paper II* describes the attempts at developing a full agonist 5-HT_{1B} PET radioligand. Neither of the agonists selected were able to enter the brain and bind to 5-HT_{1B} receptors in a significant amount. Because of the poor performance of the full agonists, a highly agonistic 5-HT_{1B} PET radioligand, [^{11}C]AZ12175002, which has previously been developed and tested in baseline PET measurements, was selected for an initial pilot study with a comparison of three PET radioligands with differing intrinsic activity in *paper III*. The study was able to show all three radioligands, [^{11}C]AZ10419369, [^{11}C]AZ10419096 and [^{11}C]AZ12175002, are dose-dependently sensitive towards fenfluramine induced changes in endogenous 5-HT concentrations. A framework for an extended study was established with regards to dose levels and multiples number of PET measurements needed at each dose. *Paper IV* describes the development and initial characterization of [^{18}F]AZ10419096, a fluorine-18 labeled version and identical structure of [^{11}C]AZ10419096, showing high binding potential and specific binding in blocking PET measurement.

In conclusion, this thesis describes the development of novel carbon-11 labelled PET radioligands with differing intrinsic activity and the development of a fluorine-18 labelled PET radioligand for future studies of the 5-HT_{1B} receptors in brain.

LIST OF SCIENTIFIC PAPERS

I. **Anton Lindberg**, Sangram Nag, Magnus Schou, Akihiro Takano, Junya Matsumoto, Nahid Amini, Charles S. Elmore, Lars Farde, Victor W. Pike, Christer Halldin. (2017). [^{11}C]AZ10419096 – a full antagonist PET radioligand for imaging brain 5-HT$_{1B}$ receptors. *Nuclear Medicine and Biology,54,* 34-40.

II. **Anton Lindberg**, Shuiyu Lu, Sangram Nag, Magnus Schou, Jeih-San Liow, Sami S. Zoghbi, Michael P. Frankland, Robert L. Gladding, Cheryl L. Morse, Akihiro Takano, Nahid Amini, Charles S. Elmore, Yong Sok Lee, Robert B. Innis, Christer Halldin, Victor W. Pike. (2019). Synthesis and evaluation of two new candidate high-affinity full agonist PET radioligands for imaging 5-HT$_{1B}$ receptors. *Nuclear Medicine and Biology, 70,* 1-13.

III. **Anton Lindberg**, Ryosuke Arakawa, Tsuyoshi Nogami, Sangram Nag, Magnus Schou, Chandrasekhar Mushti, Rolf Swenson, Charles S. Elmore, Lars Farde, Victor W. Pike, Christer Halldin. Evalution of endogenous 5-HT release on PET radioligand binding to 5-HT$_{1B}$ receptors: comparison of three PET radioligands with differing intrinsic activity. *Manuscript.*

IV. **Anton Lindberg**, Sangram Nag, Magnus Schou, Rysuke Arakawa, Tsuyoshi Nogami, Mohammad Mahdi Moein, Charles S. Elmore, Victor W. Pike, Christer Halldin. Development of a ^{18}F-labeled PET radioligand for imaging 5-HT$_{1B}$ receptors: [^{18}F]AZ10419096. *Manuscript.*

CONTENTS

List of abbreviations

5-HT ..... Serotonin

5-HT_{1B} ..... Serotonin receptor subtype 1B

5-HTT ..... Serotonin transporter

A_m ..... Molar activity measured in GBq/µmol

B_{max} ..... Receptor density

BBB ..... Blood brain barrier

BCRP ..... Breast cancer resistant protein

BP ..... Binding potential

CNS ..... Central nervous system

EC_{50} ..... Agonist concentration at 50% effect

EOS ..... End of synthesis

Ex vivo ..... "Out of the living"

f_P ..... Plasma free fraction

GABA ..... γ-Aminobutyric acid

GDP ..... Guanosine diphosphate

G-protein ..... Guanine nucleotide binding protein

GPCR ..... G-protein coupled receptor

GTP ..... Guanosine triphosphate

HPLC ..... High performance liquid chromatography

HRMS ..... High resolution mass spectrometry

HRRT ..... High resolution research tomograph

IC_{50} ..... Inhibitor concentration at 50% inhibition

ID ..... Injected dose

In vitro ..... "Within the glass"

In vivo ..... "Within the living"

i.v. ..... Intravenous

K_D ..... Disassociation constant at equilibrium

K_I ..... Inhibition constant.

KO ..... Knock-out

log*D* ..... Logarithm of partition coefficient of 1-octanol/water at pH 7.4

LG ..... Leaving group

MAO ..... Monoamine oxidase

MRI ..... Magnetic resonance imaging

NHP ..... Non-human primate

NIDDK ..... National Institute of Diabetes and Digestive and Kidney diseases

NIH ..... National Institutes of Health

NIMH ..... National Institute of Mental Health

NMR ..... Nuclear magnetic resonance

OTf ..... Triflate, trifluoromethanesulfonate

PET ..... Positron emission tomography

P-gp ..... Permeability-glycoprotein

RCY ..... Radiochemical yield

ROI ..... Region of interest

S_N2 ..... Bimolecular nucleophilic substitution

S_NAr ..... Nucleophilic aromatic substitution

SRRI ..... Selective serotonin reuptake inhibitor

SRTM ..... Simplified reference tissue model

SUV ..... Standardized uptake value

TBA ..... tert-Butylamine

THF ..... Tetrahydrofuran

TOI ..... Time of injection

V ..... Volume of distribution

1 INTRODUCTION

1.1 POSITRON EMISSION TOMOGRAPHY

Imaging techniques, such as magnetic resonance imaging (MRI) and X-ray, have become an important aspect of both biochemical research and medical treatment. While those techniques are useful they can only visualize structures and processes on an anatomical scale. Positron emission tomography (PET) is a non-invasive imaging technique that can study biological processes in living subjects (1,2). PET can be used for studying receptor occupancy, metabolism, biodistribution and to identify mechanisms of a disease without any pharmacological consequences and has become a useful tool in pharmaceutical research and development (3-5). A key aspect of PET imaging is micro-dosing, i.e. a dose well below what could be considered pharmacologically active (6). This means PET can be used as an early evaluation of new potential pharmaceutical drugs before setting up expensive clinical trials (7). PET has been used to study neurotransmitters in brain since the 1980s (8).

Table 1. Physical data of some of the more commonly used radio-isotopes in PET (2).

Element	**O**	**N**	**C**	**F**
Radioisotope	**^{15}O**	**^{13}N**	**^{11}C**	**^{18}F**
Half-life (min)	**2.04**	**9.96**	**20.4**	**109.7**
Decay product	**^{15}N**	**^{13}C**	**^{11}B**	**^{18}O**
Maximal positron energy (MeV)	**1.74**	**1.19**	**0.97**	**0.64**
Penetration distance* (mm)	**8**	**5**	**4**	**2**

* Maximum distances in water.

PET utilizes cyclotron generated positron-emitting short-lived isotopes of elements naturally occurring in biochemically active molecules, such as carbon, nitrogen, oxygen and fluorine (**Table 1**) (9, 10). A cyclotron is a particle accelerator using a magnetic field to accelerate a small particle into a target containing starting material for a nuclear reaction generating radioisotopes. These isotopes are incorporated in a biologically active molecule that is administered, usually intravenously, to the subject and distributed in the living tissue according to the pharmacokinetics of the biomolecule. The short-lived isotopes incorporated in the biomolecule decays by emitting a positron that annihilates upon collision with an electron, producing two gamma (γ) rays of 511 keV radiating in 180° away from the point of annihilation (**Figure 1**). Depending on the energy of the emitted positron, the positron will travel between 1-8 mm before annihilation, lower energy means shorter distance. The distance is also dependent on the density of the medium the positron is travelling through. The detection of the gamma rays is based on a "coincidence event", i.e. two γ rays hitting the detectors on opposite sides of the subject within a defined time allowing for the determination of the location of the annihilation(11). Quantitative image reconstruction can then produce visualization of

where in the subject the radioligand has accumulated and generate a tomographic image (12). The data can also be represented as time activity curves which displays the accumulation of radioactivity in a region over the time of the PET measurement (13). This allows for the quantification of the PET data that can be used to describe relative regional distribution of the PET radiotracers, binding to targets and blocking or displacement thereof.

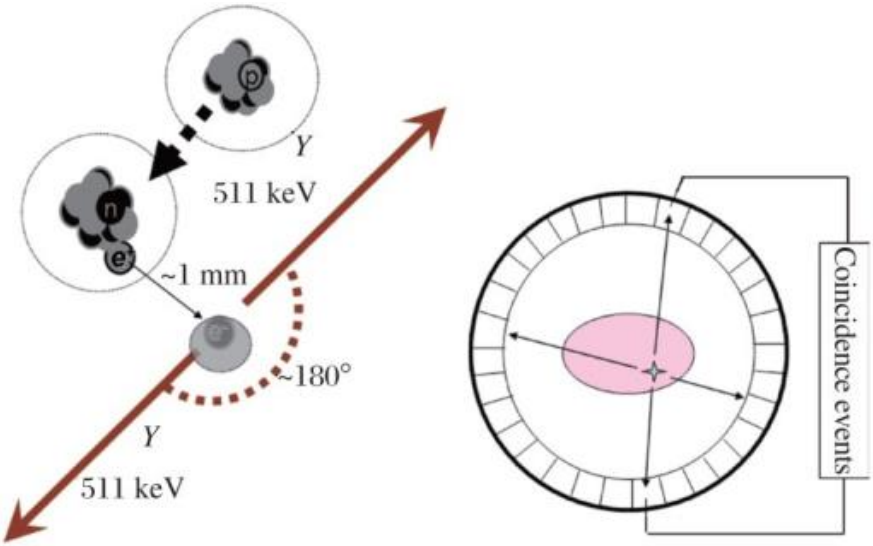

Figure 1. Positron decay of a neutron-deficient radionuclide and principle of positron emission tomography (14). A positron is emitted from the radionuclide and annihilates upon collision with an electron giving of two 511 keV γ-rays which can be detected by a PET camera

1.2 CNS PET RADIOLIGAND DEVELOPMENT AND EVALUATION

Designing PET radioligands for application in the central nervous system (CNS) requires considerations of several factors and the resources to perform biological assays to evaluate a large number of potential molecules. PET radioligand development has a lot in common with pharmaceutical drug development. Early stage development of pharmaceuticals tend to follow Lipinski's rule: 5 or less hydrogen bond donors; less than 10 hydrogen bond acceptors; molecular weight below 500; clog*P* below 5 (15). These rules are considered to be limited to oral administration, which is seldom used in PET measurements but still relevant for PET radioligands as many of them start of as potential pharmaceuticals. Lately these rules have been shown to be only moderately effective predictors even for pharmaceuticals but are still being used as initial guidelines (16, 17). A CNS PET radioligand does have a slightly different purpose than a pharmaceutical drug. The role of any CNS PET radioligand is to give a clear PET image in a micro-dose paradigm from which data can be extracted. For a drug-like molecule or pharmaceutical, to be suitable as a CNS PET radioligand it needs to have high binding affinity relative to the target receptor concentration (B_{max}). Inhibition constant (K_I) and dissociation constant (K_D) are both used to describe affinity but are measured differently. K_D describes a ratio of free ligand and receptor to receptor-ligand complex at an equilibrium. K_I describes a ligands ability to competitively inhibit the binding of a second ligand, an

endogenous neurotransmitter for example. A target receptor with low B_{max} requires a radioligand with higher affinity than a radioligand for a target receptor with higher B_{max} (18). They also need to display high selectivity against binding to other targets, the ability to pass the blood brain barrier (BBB) and not produce BBB-crossing radiometabolites (4, 19). The PET radioligand needs to bind specifically to the target receptor, a PET radioligand with higher non-specific binding will be difficult to use in further studies. The non-specific binding refers non-saturable binding such as adherence to fatty tissue in brain.

1.2.1 Binding potential

The relationship between K_D and B_{max} can be seen as a general definition of radioligand binding potential (*BP*) as described in the equation 1.

$$\boldsymbol{BP = B_{max}/K_D} \quad (1)$$

BP is further described using volumes of distributions in comparison to different reference concentrations (20). Volume of distribution in PET refers to the concentration of a radioligand in a specific region divided by the concentration of the radioligand in blood plasma. The volume of distribution in the target region (V_T) is compared to the volume of distribution in a reference compartment (V_{ND}) to quantify specifically bound radioligand. Non-displaceable binding potential (BP_{ND}) is the ratio of specifically bound radioligand to non-displaceable radioligand in a reference region with negligible receptor density. f_{ND} refers to the fraction of radioligand that is non-displaceable in brain as described in equation 2.

$$\boldsymbol{BP_{ND} = f_{ND}B_{avail}/K_D = (V_T - V_{ND})/V_{ND}} \quad (2)$$

Free plasma binding potential (BP_F) is the ratio specifically bound radioligand to the concentration of unbound radioligand in plasma where f_P refers to the fraction of unbound radioligand in plasma as described in equation 3.

$$\boldsymbol{BP_F = B_{avail}/K_D = (V_T - V_{ND})/f_P} \quad (3)$$

Total plasma binding potential (BP_P) is the ratio of specifically bound radioligand to combined bound and unbound radioligand in plasma as described in equation 4.

$$\boldsymbol{BP_P = f_P B_{avail}/K_D = V_T - V_{ND}} \quad (4)$$

All *BP* values describes the difference between specific binding and non-specific binding and are valuable in further studies regarding occupancy and competitive displacement (21). BP_F and BP_P requires arterial blood sampling during the PET measurement in order to quantify f_P and the specific binding in brain. BP_{ND} can be calculated without any blood sampling.

1.2.2 Occupancy

This thesis has focused on receptor occupancy, which can be assessed by challenge from endogenous ligand or by blocking of the receptor binding site with a competitive unlabeled compound (20). In both cases the general idea is to compare the amount of binding sites

available to the radioligand with and without competition. The competition can come from an unlabeled compound administered prior to the radioligand (pretreatment) or an unlabeled compound administered after the radioligand has achieved specific binding in brain (displacement). Displacement can only occur if the radioligand binds reversibly to the receptor (18).

1.2.3 Brain uptake

Lipinski's rule mentions lipophilicity below 5, measured in clog*P*, a calculated value. A more relevant measurement is log$D_{7.4}$, a measured relative distribution of a compound between an organic phase, octanol, and an aqueous phase at physiological p*H*, where a more lipophilic compound will favor the organic phase. Usually a log$D_{7.4}$ value of 1-3 is desired. A higher log$D_{7.4}$ value leads higher non-specific binding to the fatty tissue in brain and makes it difficult to appreciate receptor-bound radioligand. A higher log$D_{7.4}$ also increases the adherence to protein in the blood and results in a smaller fraction of radioligand free in plasma. Lipophilicity also impacts the ability of a radioligand to pass through the BBB via passive diffusion (19). Hydrophilic compounds (log$D_{7.4}$ < 1) have lower ability to passively diffuse through the fatty layer of the BBB and tend to stay in the aqueous blood plasma. Polar surface area and formal charge at physiological p*H* affects the ability of a compound to passively diffuse through the BBB. If a molecule has a pK_a value above or below physiological p*H* it will be ionized to an increasing extent and be more unlikely to pass through the BBB. Brain uptake is also affected by efflux transporter protein such as P-glycoprotein (P-gp) or breast cancer resistant protein (BCRP) that will actively transport molecules out through the BBB (22, 23). A useful CNS PET radioligand cannot be a high-affinity substrate for such efflux pumps.

1.2.4 Radiometabolism

Almost all biochemical compounds are susceptible to metabolism *in vivo*, usually by enzymes in the liver (24). Some metabolism can also occur in the brain. Any radio-metabolite that has the ability to cross the BBB or is produced in brain will confound the overall quantification of a PET measurement. Determination of the amount of the radiometabolites compared to parent compound is necessary to identify the nature of the radioactive accumulation in brain (25). Blood sampling during a PET measurement allows for determination of the amount of radiometabolites as well as the amount of radioligand bound to blood plasma protein (26). Radioligand bound to blood plasma protein will not be able to pass through the BBB and bind to the intended target in brain (18).

1.3 PET RADIOCHEMISTRY

Due to the limited half-life of positron emitting radionuclides, the incorporation of the radionuclide must be done at a late stage of the total synthesis with the ability to isolate the radioligand from any reagents or by-products as well as formulate in an appropriate solution for administration (27, 28). To evaluate this process, a few aspects are important:

Radiochemical yield. Radiochemical yield (*RCY*) is a term used to describe the efficiency of a synthesis or process. An accurate descriptions of *RCY* compares the radioactivity at the start of the process or synthesis with the amount of radioactivity of the desired product, decay-corrected for the time between the start and finish of the synthesis or process.

Radiochemical purity. Radiochemical purity describes the amount of the radioactivity in a sample that originates from one source, expressed as a percentage. Radiochemical purity does not take into consideration presence of chemical impurities that do not contribute to the radioactivity.

Molar activity. Molar activity (A_m), previously often referred to as specific activity, describes the radioactivity in a sample compared to the total amount of labeled and unlabeled compound in a sample. A_m is not constant but decreases with the half-life of the radionuclide used and is given in reference to specific time, such as end of synthesis (EOS) or time of injection (TOI).

1.3.1 Carbon-11 chemistry

Cyclotron generated carbon-11 is produced via the nuclear reaction $^{14}N(p,\alpha)^{11}C$ and depending on the gas mixture in the target; either $[^{11}C]CH_4$ (nitrogen/hydrogen) or $[^{11}C]CO_2$ (nitrogen/oxygen) is produced. Both carbon species can then be transformed to various useful ^{11}C-containing reactants (**Figure 2**). These in turn give rise to an array of product classes e.g., [^{11}C]Carbonyl compounds like acids, amides, esters and ketones from $[^{11}C]CO_2$ (29, 30), [^{11}C]CO (31, 32), and [^{11}C]HCN (33, 34), [^{11}C]Ureas from $[^{11}C]CO_2$ via isocyantes (35), [^{11}C]*N*-methyl and [^{11}C]*O*-methyl compounds from $[^{11}C]CH_3I$ (36, 37), and $^{11}C]CH_3OTf$(38, 39) and [^{11}C]thiocarbamates can be synthesized from $[^{11}C]CS_2$ (40).

Cyclotron produced $[^{11}C]CH_4$ tends to have higher A_m than $[^{11}C]CO_2$ due to less risk of contamination from atmosphere. ^{11}C-Carbonylation using [^{11}C]CO and ^{11}C-methylation using $[^{11}C]CH_3OTf$ are the methods of carbon-11 incorporation used in this thesis.

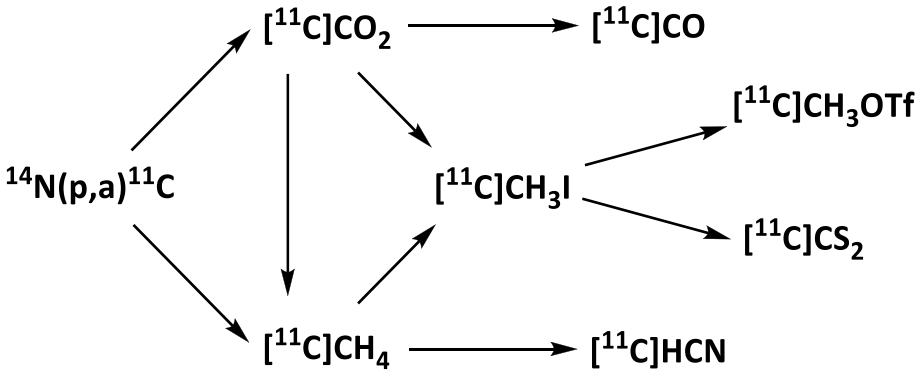

Figure 2. Possible routes for conversion of cyclotron-produced C-11 into reactive species used in PET radiochemistry.

^{11}C-Carbonylation. Cyclotron generated $[^{11}C]CO_2$ is the starting point for all ^{11}C-carbonylation chemistry utilized in PET chemistry. $[^{11}C]CO_2$ can be used directly in synthesis of [^{11}C]carboxylic acids and derivatives like [^{11}C]esters and [^{11}C]amides by reacting the $[^{11}C]CO_2$

with an appropriate organometallic compound (Mg, Li) and reducing agent (amine, alcohol or water) (41, 42). [*carbonyl*-^{11}C]Carboxylic acids, esters and amides have also been synthesized starting from boronates with CuI catalyst (43).

Conversion of [^{11}C]CO_2 to [^{11}C]CO can be done through passing the [^{11}C]CO_2 through a heated oven containing zinc (400°C) or molybdenum (850°C). The zinc method generally provides better conversion than molybdenum but molybdenum has been shown to be more reliable (44, 45). [^{11}C]CO can also be produced through a two-step conversion with lithium triethylborohydride and subsequent decomposition (46). Most [^{11}C]CO chemistry utilizes transition metal catalysis (Pd, Ni for example), according to methodologies first developed by Heck et al (47, 48). These methods allows for the synthesis of a carbonyl group starting from an aryl/vinyl-halide or pseudo-halide and the appropriate amine or alcohol depending on whether an ester or amide is desired. The aryl-halide first undergoes an oxidative addition to the metal complex followed by a reaction with carbon monoxide and finally a reductive elimination by the amine/alcohol to regenerate the metal-ligand complex and yield the desired product. This sequence is referred to as a catalytic cycle. One limitation with ^{11}C-carbonylation is the poor trapping of the gaseous [^{11}C]CO_2 or [^{11}C]CO in organic solvents. Recent developments in microfluidic reactors attempt to combat this by allowing for a finer distribution of gas in solvent (49, 50).

^{11}C-Methylation. [^{11}C]CH_3I or [^{11}C]CH_3OTf for ^{11}C-methylation reactions can be produced in a few different ways; [^{11}C]CO_2 can be converted into [^{11}C]CH_3I in two different ways (a "wet" procedure and a gas phase procedure) as well as cyclotron produced [^{11}C]CH_4 being converted to [^{11}C]CH_3I (51). In the "wet" method [^{11}C]CO_2 is bubbled through a vessel of $LiAlH_4$ in THF or Et_2O reducing [^{11}C]CO_2 to lithium [^{11}C]methoxide, which when treated with water gives [^{11}C]methanol. Addition of hydroiodic acid gives the desired [^{11}C]CH_3I (52). In the gaseous method [^{11}C]CO_2 is pushed in to an oven with nickel and under pressure is reduced in presence of hydrogen gas from [^{11}C]CO_2 to [^{11}C]CH_4, which can then be converted into [^{11}C]CH_3I in presence of I_2 at 720°C. If using cyclotron produced [^{11}C]CH_4 only the last step is needed (36). [^{11}C]CH_3I can be further converted into the more electrophilic [^{11}C]CH_3OTf by passing through an column containing silver triflate at 160-190°C.

1.3.2 Fluorine-18 chemistry

Fluorine is not present in endogenous compounds and only in a fraction of pharmaceutical drugs, but due to its small size it can be incorporated in biologically active compounds by replacing hydrogen or hydroxyl groups with fluorine. As in [^{18}F]2-fluoro-2-deoxy-D-glucose ([^{18}F]FDG), where a hydroxyl group is replaced by fluorine-18. [^{18}F]FDG has long been used in cancer diagnostics (53). Cyclotron generated fluorine-18 can be produced via two different nuclear reactions, ^{18}O(p,n)^{18}F and ^{20}Ne(d,α)^{18}F (54-56). Both reactions can be utilized to produce [^{18}F]F_2 gas, which can be used in electrophilic labelling reactions. For nucleophilic reaction, [^{18}F]F^- is needed and can only be produced through the ^{18}O(p,n)^{18}F reaction. One major difference between using [^{18}F]F_2 and [^{18}F]F^- is that [^{18}F]F_2 will give a lower A_m because F_2 gas is added to the target for more effective release of radioactivity from the target. This

process is referred to as “carrier added”. Which is partly why $[^{18}F]F^-$ is more utilized and a wide scope of labeling strategies have been developed (57, 58).

Electrophilic and radical radiofluorination. $[^{18}F]F_2$ is the most common source for electrophilic and radical fluorination and can be used directly or to generate secondary fluorination reagents. Xenon difluoride $[^{18}F]XeF_2$, can be produced in a reaction of $[^{18}F]F_2$ with xenon in presence of nickel (59), and also from $[^{18}F]F^-$ (60). *N*-[^{18}F]fluorobenzenesulfonimide ([^{18}F]NFSI), is a useful reagent for fluorination reactions of ethers, aldehydes and silylalkenes (61). One of the most common electrophilic fluorination reagents, 1-chloromethyl-4-fluoro-1,4-diazoniabicyclo [2,2,2]octane bis(triflate), Selectfluor, has been labeled from $[^{18}F]F_2$ to perform late-stage radiofluorinations (62). Because of the limitations on A_m when using $[^{18}F]F_2$, strategies for umpolung reactions using $[^{18}F]F^-$ to perform electrophilic fluorination are being developed (63, 64).

Nucleophilic radiofluorination. Nucleophilic aromatic substitution reaction (S_NAr) and/or nucleophilic substitution 2 (S_N2) reactions are the most common way of using $[^{18}F]F^-$. $[^{18}F]F^-$ is a useful nucleophile on its own but it’s generally produced from [^{18}O]water. Water stabilizes the $[^{18}F]F^-$ anion through hydrogen bonds and steps to activate $[^{18}F]F^-$ by removal of [^{18}O]water are needed. Target water containing $[^{18}F]F^-$ ions is passed through a QMA Seppak cartiridge, an ion exchange column, that retains ions while eluted with water (65, 66). The trapped $[^{18}F]F^-$ ions are eluted with aqueous acetonitrile solution containing a counter anion and a phase transfer catalyst, such as potassium carbonate and kryptofix 2.2.2. (67). Subsequent azeotropic evaporation of the water with acetonitrile improves the reactivity of the $[^{18}F]F^-$ ion. With almost all water removed kryptofix 2.2.2. isolates the $[^{18}F]F^-$ anion from the postassium cation and improves the reactivity of it by charge separation. $[^{18}F]F^-$ can then be used as nucleophile in a S_NAr to make [^{18}F]fluoroarenes, providing the aromatic ring is electron deficient with a suitable leaving group (LG) and an electron withdrawing substituent in either *ortho*- or *para*-position (68). The most common LGs in radiofluorination S_NAr reaction are nitro and trimethylammonium groups but halides have also been used (69, 70). Because of the limitation to activated aromatic rings and suitable LGs, new techniques have been needed to enable late-stage fluorination of pharmacologically active compounds. These include the use of iodonium salts, transition metal catalysts, and prosthetic group labeling (71-73).

1.4 G-PROTEIN COUPLED RECEPTORS

G-protein coupled receptors (GPCRs) are membrane proteins that mediate cellular signaling over cell membranes.(74) All GPCRs have a similar structure of seven subunits spanning the cell membrane The G-protein itself consists of three subunits (α, β, γ), where the α-subunit binds to the receptor. The receptor binds to a neurotransmitter and activates the G-protein on the other side of the membrane (75). GPCRs are not permanently coupled to the G-protein but exist in a series of conformational states with various affinity to ligands and efficacy upon binding (76). How many conformations exist and how these conformational changes occur is

unclear and may vary between different GPCRs. Complex models have been developed that also show the role of guanidine nucleotides (GDP/GTP) in activating G-protein to couple and uncouple from the receptor. Binding of an agonist is not enough to activate the GPCR but is dependent on the relative fraction of GTP and GDP bound to the G-protein. It has also been suggested that the binding of a ligand itself will conform and stabilize the GPCR in one state (77-79). In all these models it is generally considered that the G-protein coupled receptor is the agonist high affinity state, but the exact sequence of activation may vary (80).

Several *in vitro* studies on GPCRs in the serotonergic system have shown that agonist binding is more affected by changes in receptor affinity states and that only a fraction of the total GPCR population is in an agonist high affinity state. These studies show a distinct dual affinity when evaluating the GPCR with an agonist, while an antagonist only shows one affinity (81-83). While the exact distribution between agonist high affinity and low affinity receptor complexes differ between receptor subtypes, the general idea is that endogenous substrate and agonist will almost exclusively bind to the high affinity state whereas an antagonist will bind more indiscriminately to both states (**Figure 3**).

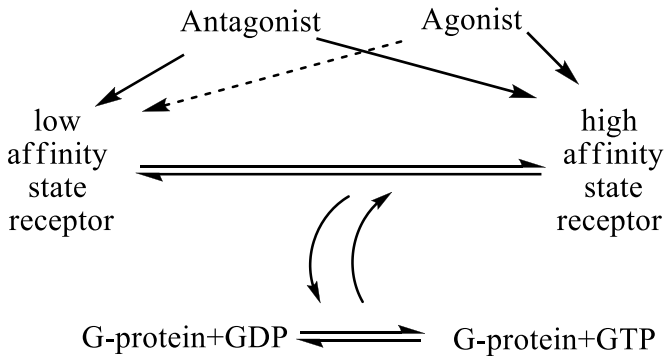

Figure 3. Simplified schematic view of antagonist/agonist interaction with GPCRs. The G-protein coupled receptor is generally considered the high affinity form of the receptor but it is not clear whether the coupling itself activates the receptor. Agonist binds with lower affinity to the low affinity receptor, whereas antagonist bind with equal affinity to both.

PET studies on the dopaminergic system have shown higher displacement of an agonist radioligand than an antagonist radioligand by endogenous neurotransmitter, but this has not yet been replicated for the serotonergic system (84). 5-HT_{1B} receptors have been shown to exist in an equilibrium of at least two separate affinity states, but it has not been determined how this equilibrium affects the binding of agonists and antagonists *in vivo* and if it can be quantified using PET (85).

1.5 SEROTONERGIC SYSTEM

Serotonin (5-HT) is a neurotransmitter and plays a vital role in several higher brain functions, such as emotion and cognition (86). The serotonergic system spans the entire CNS and much of the rest of the body, with 7 receptor families further divided into 14-16 subtypes of receptors

that exhibit different regional densities and physiological functions (87-89). 5-HT is a small and polar molecule that cannot pass the BBB but is instead synthesized in serotonergic neurons starting from the amino acid L-tryptophan. Tryptophan hydroxylase converts L-tryptophan first into 5-hydroxy-tryptophan (5-HTP), which can pass through the BBB, 5-HTP is subsequently decarboxylated into 5-HT and then stored and transported in vesicles along neurons to the synapses to activate the different physiological actions. Reuptake of 5-HT into the neuron cell is done by serotonin transporter channels (5-HTT). 5-HT is degraded by monoamine oxidase (MAO) to 5-hydroxyindoleacetic acid, which can be cleared out of the body through the kidneys (**Figure 4**). 5-HTT is an interesting target for inhibition with selective serotonin reuptake inhibitors (SSRI), where the aim is to prolong 5-HT signaling along the neuropathic system and has been studied with PET (90). MAO is further divided into MAO-A and MAO-B, with PET radioligands developed for both enzymes (91). Synaptic concentrations need to be regulated to maintain normal brain function. This happens both through activation and de-activation of release and uptake of 5-HT (92, 93). The 5-HT receptors function both as autoreceptors and heteroreceptors; autoreceptors regulate reuptake and continued release on the presynaptic neuron, heteroreceptors continue the signal post-synapse (94). Comparisons can be made with dopamine as they are both monoamine neurotransmitters active in the CNS and both the dopaminergic and serotonergic systems have been studied using PET (95).

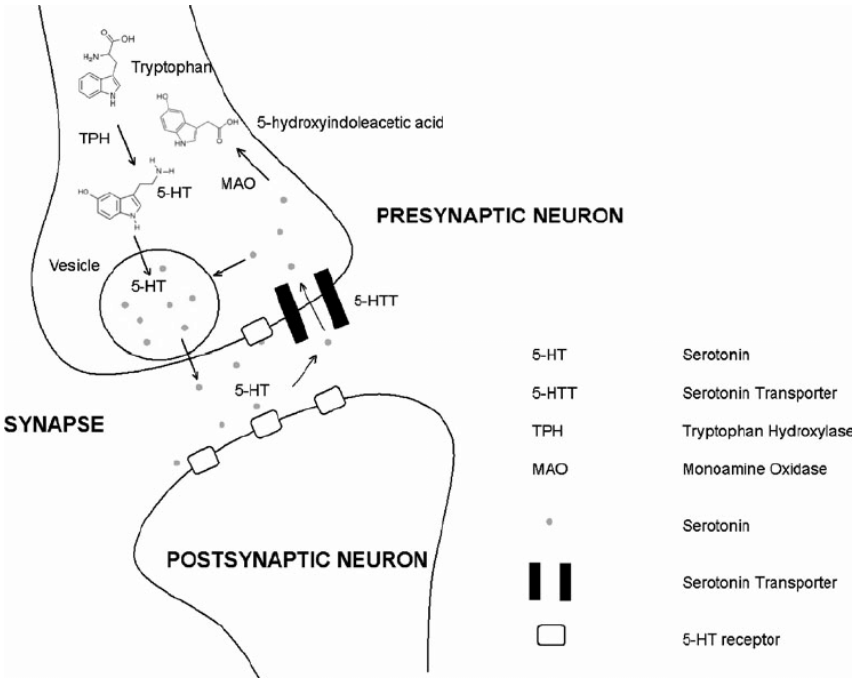

Figure 4. Schematic view of the serotonergic cycle in the neuron and synaptic cleft (96). L-tryptophan is converted into 5-HT, released through vesicles to the synapse and reuptake goes through the 5-HTT channels and subsequent degradation via MAO.

1.5.1 5-HT$_{1B}$ receptors

The 5-HT$_{1B}$ receptor is most widely expressed in the occipital cortex and globus pallidus in humans. In rodents the expression is slightly different with low expression in cerebrum but higher in the substantia nigra (97, 98). 5-HT$_{1B}$ was originally thought to be a substructure of

the human 5-HT_{1D} receptor but has since been reclassified as a structurally unique 5-HT receptor (99). The 5-HT_{1B} receptor expressed in rodent is structurally different from the human receptor, which leads to some drugs like sumatriptan having little to no effect in rodent but evident effect in humans whereas propanolol has the opposite species preference (100). The 5-HT_{1B} receptor is implicated in depression, anxiety and migraine and is an interesting target for PET studies focusing on changes in endogenous serotonin concentrations (101).

5-HT_{1B} receptors are present on neurons for other neurotransmitters, such as γ-aminobutyric acid (GABA), dopamine and acetylcholine as well as 5-HT. It is expressed as both an autoreceptor presynaptically and as a heteroreceptor postsynaptically (100). The 5-HT_{1B} receptor couples to α-subunit of a G-protein that is negatively linked to adenylate cyclase, meaning that when the 5-HT_{1B} receptor is activated it deactivates the cyclase enzyme. When expressed as an autoreceptor the adenylate cyclase controls further release of 5-HT into the synaptic cleft (102). A 5-HT_{1B} agonist or endogenous 5-HT will therefore inhibit further release of 5-HT, whereas an antagonist will allow further release and initially increase the 5-HT concentration in the synaptic cleft. 5-HT_{1B} also functions as a hetero-receptor on the receiving end of non-serotonergic neurons regulating further signaling along the receiving neuron (103, 104). Recent crystal structures of human 5-HT_{1B} receptor bound to agonist or antagonist show distinct structural changes to the receptor depending on the intrinsic activity of the ligand (105, 106). Both agonist and antagonist will form hydrogen bonds with a threonine and asparagine amino acid in the deeper part of the binding site, but agonists and endogenous 5-HT will allow one of the seven subunits to act as a "toggle switch" which has been considered to be the initial activation step of GPCRs (107).

1.5.2 5-HT_{1B} PET studies

Two PET radioligands have been developed for imaging 5-HT_{1B} receptors in brain, [^{11}C]AZ10419369 and [^{11}C]P943 (**Figure 5**) (108, 109). [^{11}C]AZ10419369 was selected from the same library of compounds used in this thesis and along with seven other candidates was evaluated in an initial PET study in monkey (110). Binding is highest in occipital cortex and globus pallidus and negligible in cerebellum. Cerebellum has been used as a reference region approximating non-specifically bound radioligand to quantify BP_{ND}. BP_{ND} is reportedly higher for [^{11}C]AZ10419369 than for [^{11}C]P943 but both of these radioligands have been shown to bind specifically to 5-HT_{1B} in monkey brain. Both have shown to have high selectivity for 5-HT_{1B} receptors over other 5-HT receptors as well as being displaceable by fenfluramine-induced changes in endogenous 5-HT concentrations (111, 112). 5-HT_{1B} is an interesting target for studying fluctuation in synaptic 5-HT concentrations using PET and [^{11}C]AZ10419369 has even shown to have a dose-dependent displacement with two separate doses of fenfluramine. Because fenfluramine is not approved for clinical studies, recent studies has been aimed at establishing protocol for 5-HT release using approved drugs (113). [^{11}C]AZ10419369 has also been used in PET studies in pig (114). [^{11}C]AZ10419096 and [^{11}C]P943 has been used to study depression and Parkinson's disease as well as migraine in clinical studies (115-118). Both [^{11}C]AZ10419096 and [^{11}C]P943 were originally described as antagonists but recently

[^{11}C]AZ10419369, at least, has been reconsidered to be a partial agonist. Since it is proposed that an agonist and antagonist PET radioligand targeting a GPCR would have differing sensitivity to completion from endogenous neurotransmitters, 5-HT$_{1B}$ could be an interesting target for such studies with the development of PET radioligands of differing intrinsic activity (101). Both current PET radioligands for 5-HT$_{1B}$ receptor imaging utilizes the shorter lived carbon-11 radionuclide. An ^{18}F-labeled radioligand would open up the research into 5-HT$_{1B}$ receptors to facilities even without a cyclotron on-site.

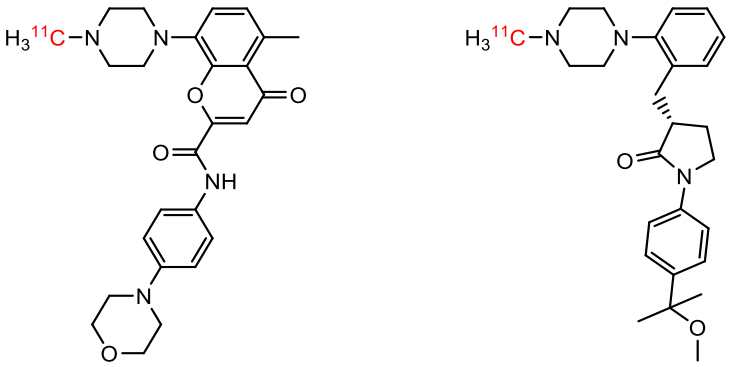

Ligand	**[^{11}C]AZ10419369**	**[^{11}C]P943**
K_I (nM)	0.4	1.2
LogD	1.3	2.3
***BP*$_{ND}$** (occipital cortex)	1.52	0.71

Figure 5. Prior to this thesis two PET radioligand has been developed to image 5-HT$_{1B}$ receptors in brain, [^{11}C]AZ10419369 and [^{11}C]P943.

2 AIMS

The overall aim of this thesis was to expand the possibilities for imaging 5-HT_{1B} receptors in brain by developing novel PET radioligands and to evaluate their ability to detect changes in endogenous 5-HT concentrations.

The specific aims of this thesis were:

1. To develop a full antagonist carbon-11 labelled 5-HT_{1B} PET radioligand, *paper I*
2. To develop a full agonist carbon-11 labelled 5-HT_{1B} PET radioligand, *paper II*
3. To evaluate if the intrinsic activity of a 5-HT_{1B} PET radioligand influences its ability to detect changes in endogenous 5-HT concentrations, *paper III*
4. To develop a fluorine-18 labelled 5-HT_{1B} PET radioligand, *paper IV*

3 MATERIAL AND METHODS

3.1 CHEMISTRY AND RADIOCHEMISTRY

A brief summary of chemistry and radiochemistry procedures used in this thesis. All precursor synthesis procedures and radiochemistry methodology are described in detail in each constituent paper.

3.1.1 Precursor synthesis

Detailed experimental procedures and methods for each precursor synthesis can be found in their corresponding papers. All intermediate, precursors, and reference compounds were isolated and analyzed with high resolution mass spectrometry (HRMS) as well as ^{1}H and ^{13}C NMR.

^{1}H (400.13 MHz) and ^{13}C (100.62 MHz) NMR spectra were recorded on an Advance 400 instrument (Bruker) at room temperature in deuterated solvents. NMR signals are reported as δ (ppm) downfield from the signal of tetramethylsilane. HRMS data (ESI-TOF) were obtained at Bioorganic Chemistry Laboratory of NIDDK (NIH). Optical rotations were measured on a P-1010 polarimeter (JASCO).

3.1.2 Carbon-11 chemistry

All radiosynthesis in *papers I*, *III* and *IV* as well as radiosynthesis of [^{11}C]AZ11895987 in *paper II* were performed exclusively at the Karolinska Institutet, Stockholm, Sweden.

Radiosynthesis of [^{11}C]AZ11136118 for *paper II* were performed exclusively at the Molecular Imaging Branch, NIMH, Bethesda, MD, USA.

^{11}C-Methylation. Radiomethylations to produce [^{11}C]AZ10419096, [^{11}C]AZ11895987 and [^{11}C]AZ12175002 were performed with the same general method: [^{11}C]CH_3OTf from cyclotron-generated [^{11}C]CH_4 was bubbled through a solution of desmethyl precursor (0.2-0.5 mg) in acetone (0.5 mL) with NaOH (6.0µL, 0.5 M). After 2 min at ambient temperature, the solution was diluted with water (3 mL) and injected onto a reverse phase ACE C-18 HPLC column (250 × 10 mm; Advanced Chromatography Technologies Ltd) using a ratio of acetonitrile in aqueous NH_4HCOOH (0.1M) appropriate for a product retention time of 8 to 12 min. Acetonitrile was removed from collected fraction by evaporation (*paper I*) or by solid phase extraction eluting with 10% w/w ethanol(*paper II and III*) and formulated in sterile saline solution.

^{11}C-Carbonylation. [^{11}C]CO generated from cyclotron produced [^{11}C]CO_2 was mixed under pressure (~3500 psi) with a mixture of Pd_2dba_3 (1.3 mg, 1.4 µmol), Xantphos (3.0 mg, 5.2 µmol) and 4-iodophenyl methanesulfonate (2.4 mg, 8.1 µmol) in THF (80 µL). After reaction at 150°C during 3 min the solution was transferred into a second reaction vessel containing

(*R*)-8-(4-Methylpiperazin-1-yl)-1,2,3,4-tetrahydronaphthalen-2-amine **(**3.2 mg, 13 µmol) and Bu_3N (10 µL, 42 µmol) in THF (50 µL). The second reaction was heated from 67°C to 100°C while THF was evaporated. The remaining residue was dissolved in acetonitrile and water before being injected onto a Luna C18 column (10 µm, 10 × 250 mm; Phenomenex; Torrance, CA) eluted with a gradient of 90-55% of 0.2% aqueous NH_4OH (p*H* = 8.5) in acetonitrile. The fraction containing [^{11}C]AZ11136118 eluated between 17 and 19 min. Acetonitrile was removed by evaporation and [^{11}C]AZ11136118 was formulated in sterile saline solution.

3.1.3 Fluorine-18 chemistry

Cyclotron produced [^{18}F]F^- ions, K_2CO_3 (1.8 mg, 13 µmol) and kryptofix 2.2.2 (4,7,13,16,21,24-hexaoxa-1,10-diazabicyclo-[8.8.8]hexacosane-K2.2.2) (9.8 mg, 26 µmol) in water (85 µL, 18 MΩ) and acetonitrile (2 mL) were eluted into a glass reaction vessel (10 mL). The solvent was removed by azeotropic evaporation with acetonitrile at 140°C under continuous nitrogen flow (70 mL/min). The borate precursor, (60 µmol), and $[Cu(OTf)_2(py)_4]$ (5 µmol) were dissolved in DMF (500 µL) and added manually to the reaction vessel. The closed reaction vessel was heated at 120°C for 10 min. The reaction mixture was then cooled to room temperature and diluted with water (3 mL) before being injection onto a reversed phase ACE C-18 HPLC column (250 × 10 mm; Advanced Chromatography Technologies Ltd). Excess [^{18}F]F^- was washed out with water over 5 min before switching to a mobile phase of 40% acetonitrile in aqueous NH_4HCOOH (0.1M) containing 0.01% sodium ascorbate. [^{18}F]AZ10419096 eluted at 12 min after changing mobile phase. Acetonitrile was removed by solid phase extraction and [^{18}F]AZ10419096 was formulated in sterile saline solution with 10% w/w ethanol.

3.1.4 Radiochemical purity and A_m analysis

Radiochemical purity of the formulated products were determined with reversed phase HPLC on either ACE 5 C18-HL column (3.9 × 300 mm, 10 µm; Advanced Chromatography Technologies Ltd) at Karolinska Institutet or a Luna C18 column (10 µm, 4.6 × 250 mm; Phenomenex) at NIMH, with eluate monitored in series for absorbance at 254 nm and radioactivity. For the analysis, the column was eluted using an optimized ratio of acetonitrile in an appropriate aqueous solution. The products were identified by their co-elution with corresponding reference samples.

A_m was the radioactivity at EOS of the radioligand (GBq) divided by the amount of the associated carrier substance (µmol). Each sample was analyzed three times by reversed phase HPLC on either ACE 5 C18-HL column (3.9 × 300 mm, 10 µm; Advanced Chromatography Technologies Ltd) at Karolinska Institutet or a Luna C18 column (10 µm, 4.6 × 250 mm; Phenomenex) at NIMH, and compared with a sample of reference compound of known concentration. The average area under the curve for the UV absorbance for each sample was compared to that of the reference sample to determine the amount of carrier substance in each sample.

3.2 PET EXPERIMENTAL PROCEDURES

All PET measurements for [^{11}C]AZ11136118 (*paper II*) were performed at the Molecular Imaging Branch, NIMH, Bethesda, MD, USA. All other PET measurements were performed at the Karolinska institutet, Stockholm, Sweden.

3.2.1 Non-human primates

Karolinska Institutet (*papers I, II, III and IV*)**.** All PET studies in non-human primates (NHP) at the Karolinska Institutet were approved by the Animal Ethics Committee of the Swedish Animal Welfare Agency (Dnr N185/14) and were performed according to the relevant guidelines of the Karolinska Institutet ("Guidelines for Planning, Conducting, and Documenting Experimental Research" (Dnr 4820/06-600) and "Guide for the Care and Use of Laboratory Animals".

Cynomolgus monkeys were supplied by Astrid Fagraeus Laboratory of the Swedish Institute for Infectious Disease Control (Solna, Sweden). Anesthesia was initiated via intramuscular injection of ketamine hydrochloride (ca. 10 mg/kg) and maintained after endotracheal intubation by administration of a mixture of sevoflurane, oxygen and medical air. The monkeys were observed continuously during the days of PET measurements. Body temperature was maintained by Bair Hugger-Model 505 and monitored with an esophageal thermometer. Heart and respiration rates were continuously monitored by using PC-VetGard ™ system. The monkey head was fixed in position throughout PET scanning. In each PET measurement a sterile physiological saline buffer solution containing the radioligand was injected intravenously during 5 s with simultaneous start of PET data acquisition. Radioactivity in brain was measured continuously for 123 min according to a preprogrammed series of 34 frames.

In pretreatment PET measurements using AR-A00002, a baseline PET measurement was followed on the same day three hours later by a second PET measurement with AR-A00002 (2.0 mg/kg) administered 30 min before of radioligand.

In displacement PET measurement using fenfluramine, a baseline PET measurement was followed on the same day three hours later by a second PET measurement with fenfluramine (1.0 or 5.0 mg/kg) administered 15 min (*paper III)* or 30 min (*paper I*) after the radioligand.

Molecular Imaging Branch, NIMH (*paper II*)**.** The PET imaging experiments in nonhuman primates at NIMH were performed in accordance with the Guide for Care and Use of Laboratory Animals and were approved by the National Institute of Mental Health Animal Care and Use Committee(119).

One single rhesus monkey (*Macaca mulatta*) was used for PET scan sessions in which the monkey was initially anesthetized with ketamine (10 mg/kg) and then maintained in anesthesia with 1.5% isoflurane. PET images of brain were acquired with a microPET Focus 220 scanner (Siemens Medical Solution; Knoxville, TN) for 90 min with scan durations ranging from 30 s

to 5 min. The position of the head was fixed using a stereotaxic frame. Electrocardiogram, body temperature, heart, and respiration rates were monitored throughout the experiments.

3.2.2 Rodents

Six rats (Sprague Dawley) were used in PET imaging experiments. The rats were anesthetized with ketamine (10 mg/kg) and then maintained in anesthesia with 1.5% isoflurane for PET scanning sessions after bolus intravenous administration of radioligand. PET images of brain were acquired with a microPET Focus 220 scanner (Siemens Medical Solution; Knoxville, TN) for 90 min. The PET data analysis was performed using PMOD (PMOD Technologies Ltd.; Zurich, Switzerland).

Three rats (Sprague Dawley) were used in ex-vivo PET measurements. Tariquidar (8 mg/kg) was injected intravenously through the penile vein 7 min before likewise injection of radioligand. The rats were anesthetized with 1.5% isoflurane in oxygen and sacrificed via thoracotomy at 30 min after injection. The brains were harvested and subsequently weighed and formulated into samples subjected to radio-analysis using radio-HPLC.

P-gp/BCRP knockout (KO) mice (Taconic Farm, Germantown, NY) were anesthetized with 1.5% isoflurane and oxygen and sacrificed via thoracotomy at 30 min after radioligand injection. Blood was drawn from the myocardium, and the forebrains and cerebella were subsequently harvested. The tissues were weighed and immediately subjected to analysis with radio-HPLC.

3.2.3 Radiometbolite analysis and plasma free fraction

Karolinska Institutet. Venous blood samples (2 mL) were obtained manually at 4, 15, 30, 60, 90, and 120 min after injection of radioligand for measurement of total radioactivity in whole blood and plasma and for radiometabolite analysis (120, 121). The concentration of parent radioligand was measured with HPLC on an ACE 5 C18-HL column (3.9 × 300 mm, 10 µm; Advanced Chromatography Technologies Ltd), after separating plasma from whole blood.

Recovery of radioactivity from the system was calculated by taking an aliquot (2 mL) of the eluate from the HPLC column and measuring and dividing it with the amount of total injected radioanalyte (decay-corrected).

Molecular Imaging Branch, NIMH (*paper II*)**.** Arterial blood samples were drawn for analysis of radiometabolites in plasma and for determination of a radiometabolite-corrected arterial input function. Samples (0.5−1 mL each) were drawn at 15-s intervals until 120 s, followed by 0.5- to 4-mL samples at 3, 5, 10, 30, 60, 90, and 120 min. The concentration of parent radioligand was measured with HPLC on an X-terra column (10 µm, 7.8 × 300 mm; Waters Corp.), after separating plasma from whole blood

Plasma free fraction (f_P). Manual blood samples for measurement of the fraction of unchanged radioligand in plasma, were obtained twice in the first 10 min, and then once every 10 min. The fraction was determined by HPLC on either ACE 5 C18-HL column (3.9 × 300 mm, 10

μm; Advanced Chromatography Technologies Ltd) at Karolinska Institutet or X-terra column (10 μm, 7.8 × 300 mm; Waters Corp.) at NIMH, with radio detection after filtration and formulation.

3.2.4 PET data analysis

T1-weighted brain MR images were manually co-registered to the average PET images and regions of interest (ROIs) were delineated manually for the whole brain, occipital cortex, globus pallidus, caudate nucleus, putamen, ventral striatum, cerebellum, frontal cortex, mid brain, thalamus, and hippocampus. Regional uptakes are reported as standardized uptake value (*SUV*) or %*SUV*, calculated as uptake (Bq/mL)/injected radioactivity (Bq) × body weight (g). Binding ratio was calculated as $SUV_{region}/SUV_{cerebellum}$ and specific binding ratio as $(SUV_{region}/SUV_{cerebellum}) - 1$.

Regional BP_{ND} were calculated by using the simplified reference tissue model (SRTM) (122). Cerebellum was used as reference region because this region has negligible density of 5-HT_{1B} receptors (123). The specific binding of radioligand to 5-HT_{1B} receptors was defined as the difference between the total radioactivity concentrations in the target brain regions and the cerebellum.

3.3 PHYSIOCHEMICAL PROPERTIES ANALYSIS

Apparent pK_a. [^{11}C]AZ11136118 was evaluated in phosphate buffer between p*H* 3.0 and 10.5 in 0.5 increments. The apparent pK_a value was determined as the p*H* value where the concentration of ionized and non-ionized [^{11}C]AZ11136118 were equal as measured by reversed phase HPLC on a X-terra column (10 μm, 7.8 × 300 mm; Waters Corp.).

Log$D_{7.4}$ determination. The relative distribution of [^{11}C]AZ11136118 between an aqueous phosphate buffer (p*H* 7.4) and 2-octanol was evaluated by radio-analysis using reversed phase HPLC on a X-terra column (10 μm, 7.8 × 300 mm; Waters Corp.). The logarithmic fraction of the compound concentration in octanol over the concentration in the aqueous buffer represents log$D_{7.4}$.

Quantum chemical calculations. The geometry and energetics of compound conformers in the presence of a water molecule were obtained with quantum chemical calculations. The geometry was refined in Gaussian 09 software (124). Each conformer represents the geometry optimized structures of the compounds in respect to enthalpy (Δ*H*), Gibbs free energy (Δ*G*), and dipole moment with the protonated *N*-methyl-piperazine. Conformer **a** has the piperazine in a stable chair conformation with the methyl-group facing the amide, conformer **b** has rotated the piperazine 180° between the piperazine and the bicyclic ring with the amide oxygen facing away from the piperazine and for conformer **c** the amide has been rotated 180° between the carbonyl and the bicyclic ring (**Figure 6**).

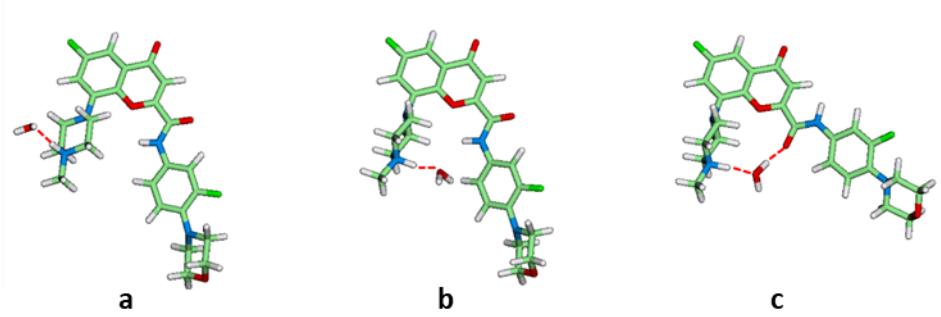

Figure 6. Geometry optimized structures of conformers of AZ11895987 (**5**) with the protonated *N*-methyl-piperazine and a water molecule. φ_1 and φ_2 are the dihedral angles centered on the respective C−N bond of **a** and C−C bond of **b**. Atoms are colored as follows: white, hydrogen; green, carbon; blue, nitrogen; red, oxygen. Dashed lines indicate the H-bonding distances (< 2.0 Å).

4 RESULTS AND DISCUSSION

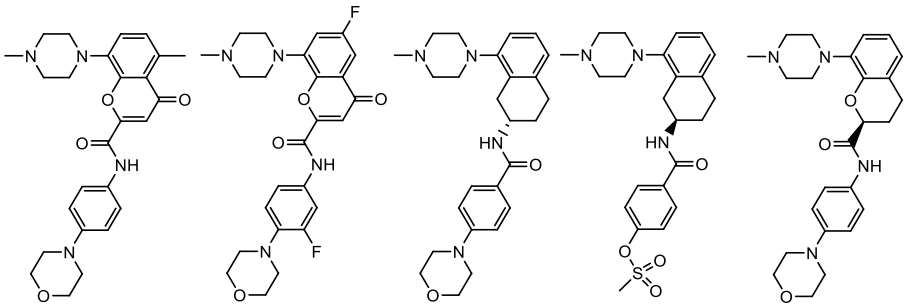

Ligand	AZ10419369	AZ10419096	AZ11895987	AZ11136118	AZ12175002
K_I (nM)	0.4	0.13	0.46	0.25	0.6
LogD	1.3	2.3	2.1	2.2	1.5
EC_{50} (nM)			0.98	0,.7	0.97
IC_{50} (nM)	50	2			
Antagonist (%)	53.2	190	-16	-3.1	18
Agonist (%)	48		113.3	112.8	77.1
Radionuclide	C-11	C-11 or F-18	C-11	C-11	C-11

Figure 7. Structures and *in vitro data* for the ligands used in this thesis. *In vitro* data provided by AstraZeneca.

4.1 FULL ANTAGONIST 5-HT_{1B} PET RADIOLIGAND (*PAPER I)*

A summary of the results from *paper I*.

AZ10419096 was identified for its favorable affinity, lipophilicity and antagonist efficacy from a library of over 3000 compounds provided by AstraZeneca (**Figure 7**).

4.1.1 Chemistry and radiochemistry

A sample of AZ10419096 was de-methylated using 1-chloroethyl chloroformate to provide the desmethyl precursor in enough yield (36%), which in turn was labeled with carbon-11 using [^{11}C]methyl triflate (**Scheme 1**). [^{11}C]Methyl triflate was added to a solution of desmethyl-AZ10419096 in acetone and NaOH with a reaction time of 2 min at ambient temperature. Purification using reverse phase HPLC followed by formulation in sterile saline gave [^{11}C]AZ10419096 in sufficient amount (1004±102 MBq), A_m (584±82 GBq/μmol) and purity (>98%) for use in PET measurement in NHP. An initial problems with radiolysis of the product was controlled by adding 0.01% sodium ascorbate to the mobile phase, which carried through to the formulated product.

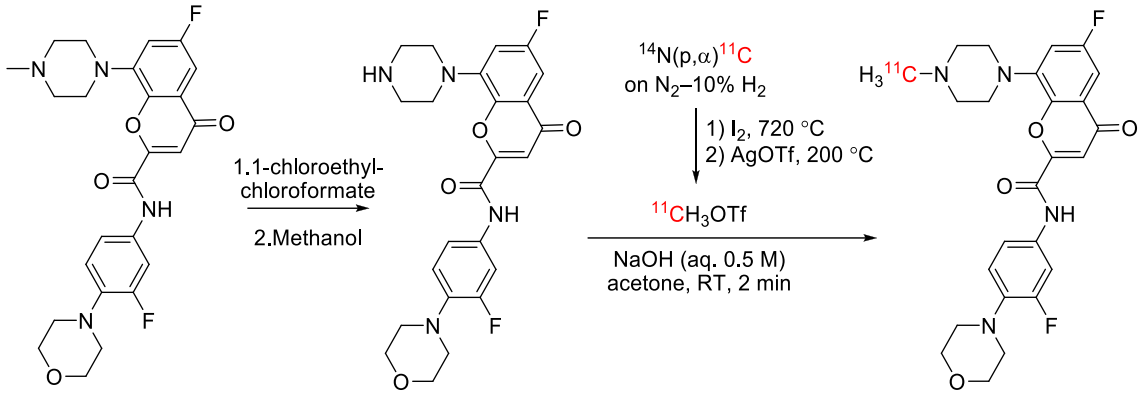

Scheme 1. Synthesis and radiolabeling of [^{11}C]AZ10419096. *1*. 1-Chloroethyl-chloroformate, DCE. *2*. Methanol, reflux. 36% yield. *Radiolabeling*. [^{11}C]CH_3OTf, NaOH, acetone.

4.1.2 PET measurements

[^{11}C]AZ10419096 was used for PET measurements in NHP. In baseline PET measurements, radioactivity entered brain quickly and reached a maximum uptake after about 10 min (**Figure 8** and **9A**). The radioactivity showed a heterogeneous distribution in brain consistent with earlier reported regional concentrations of 5-HT_{1B} receptors (97). BP_{ND} was calculated using SRTM with cerebellum as reference region to be 0.92 for occipital cortex and 1.22 for globus pallidus. In pretreatment PET measurement using AR-A000002 (2.0 mg/kg) administered 30 min prior to [^{11}C]AZ10419096, binding was blocked by 88% in occipital cortex and 90% in whole brain showing high specific binding to 5-HT_{1B} receptors in brain. (**Figure 9B**). In displacement PET measurements, fenfluramine (5.0 mg/kg) was administered 30 min after the administration of [^{11}C]AZ10419096 and 40% reduction of binding was observed in occipital cortex between 45 and 93 min, in globus pallidus only a minor reduction could be observed (**Figure 8** and **9C**).

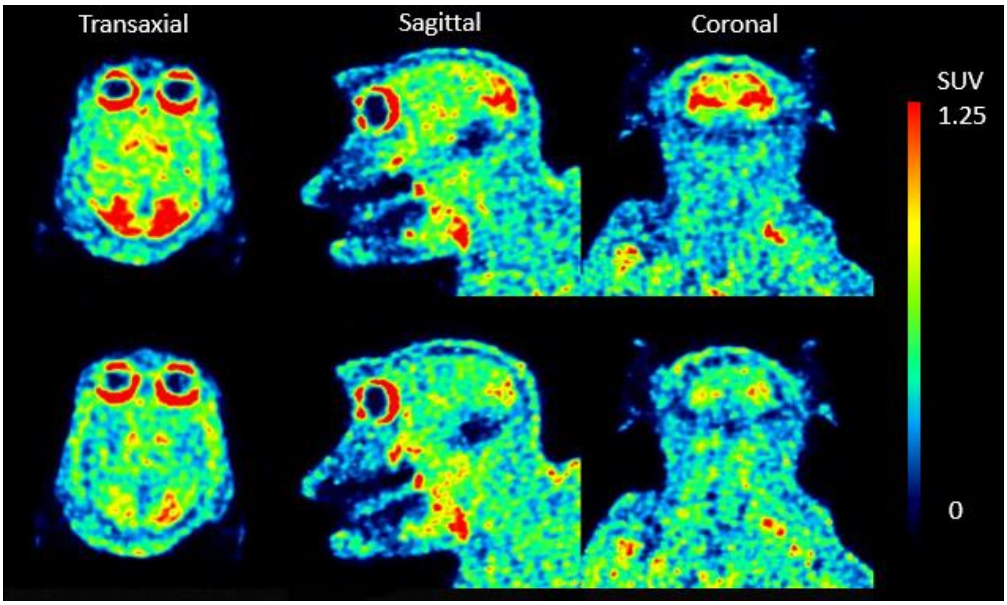

Figure 8. PET summation images (45-93 min) using [^{11}C]AZ10419096. Top row; PET summation image from baseline PET measurement, bottom row; PET summation images from PET measurement with fenfluramine (5.0 mg/kg) given 30 min after radioligand.

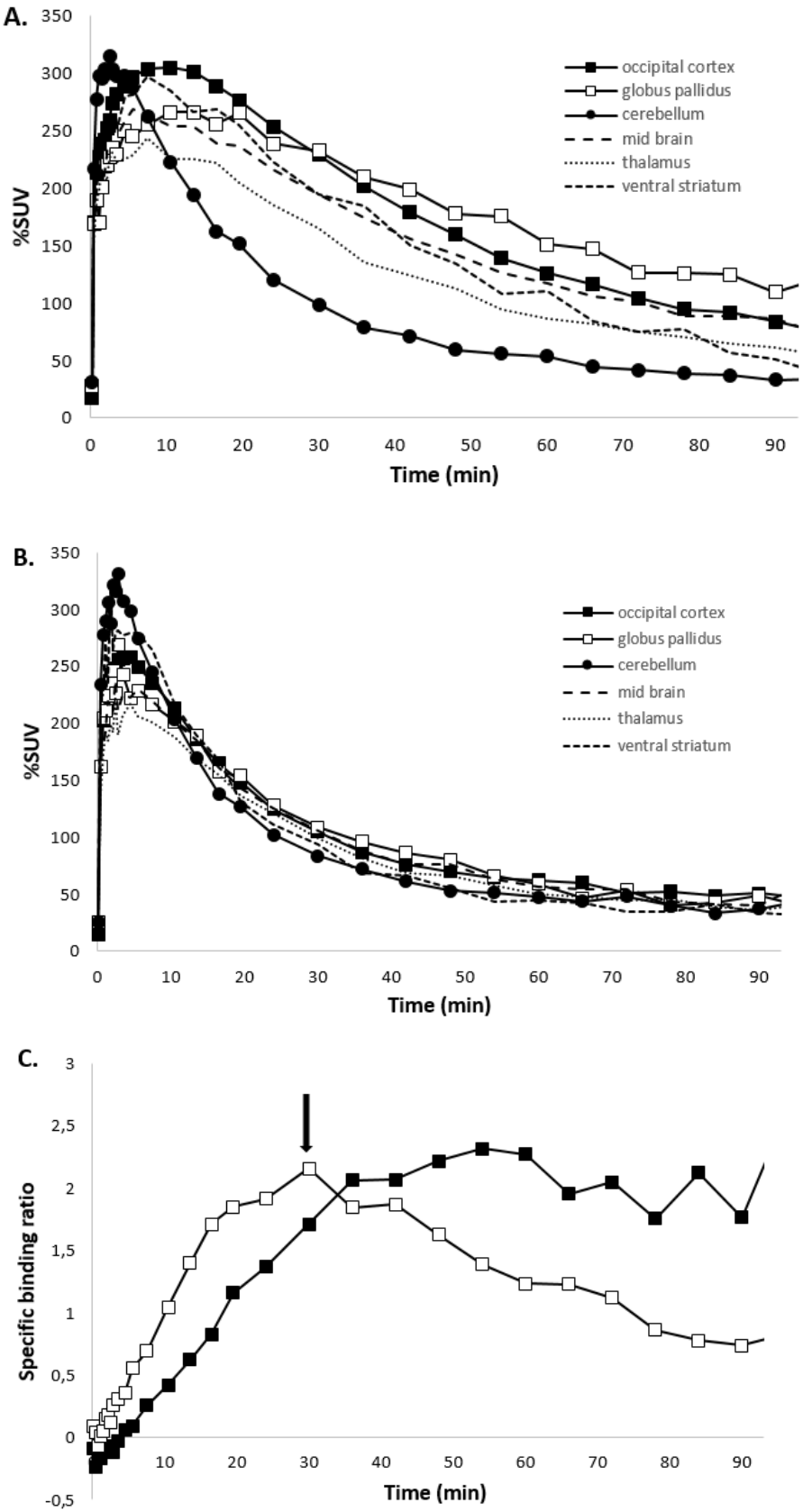

Figure 9. Time-activity curves from PET measurements (%SUV, 0-93 min) using [^{11}C]AZ10419096. **A**. Regional time-activity curves in baseline measurements, **B**. Regional time-activity curve after pretreatment with AR-A000002 (2.0 mg/kg), **C**. Specific binding ratio in occipital cortex at baseline (solid) and displacement PET measurements (hollow). Arrow denotes injection time of fenfluramine (5.0 mg/kg).

Radiometabolite analysis of plasma sampled during PET measurements showed at 60 min after administration, parent radioligand represented ~55% of radioactivity in plasma (**Figure 10**). The percentage of radioligand free in plasma was ~30%.

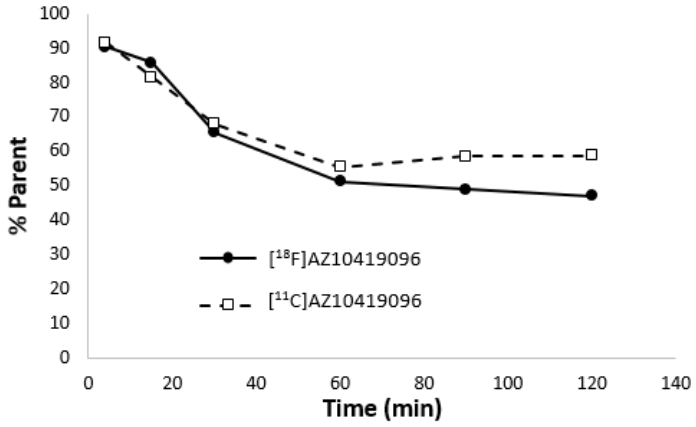

Figure 10. Radiometabolism of [^{11}C]AZ10419096 and [^{18}F]AZ10419096 in monkey baseline PET measurement. %Parent denotes percentage of radioactivity in blood plasma from unchanged radioligand.

4.1.3 Discussion

[^{11}C]AZ10419096 was selected as a full antagonist from *in vitro* data (**Figure 7**) and the initial evaluation showed high specific binding to 5-HT$_{1B}$ receptors in brain and sensitivity towards increased endogenous 5-HT concentrations induced by fenfluramine. As a full antagonist, [^{11}C]AZ10419096 could be useful in future PET studies of imaging differences in high and low affinity state 5-HT$_{1B}$ receptors.

4.2 FULL AGONIST 5-HT$_{1B}$ PET RADIOLIGANDS (*PAPER II*)

A summary of the results from *paper II*.

Both AZ11895987 and AZ11136118 were identified from the same library as AZ10419096 using the same criteria with the exception of agonist efficacy instead of antagonist efficacy.

4.2.1 Chemistry and radiochemistry

Reference samples and precursor for AZ11895987 as well as reference sample of AZ11136118 were provided by AstraZeneca.

[^{11}C]AZ11895987. [^{11}C]Methyl triflate from cyclotron-produced [^{11}C]CH_4 was bubbled through a solution of desmethyl-AZ11895987 in acetone and NaOH with a reaction time of 2 min at ambient temperature (**Scheme 2**). Purification with preparative HPLC followed by formulation in sterile saline gave [^{11}C]AZ11895987 in sufficient amount (1025 MBq), A_m (654 GBq/μmol) and purity (>98%) for use in PET measurement in NHP.

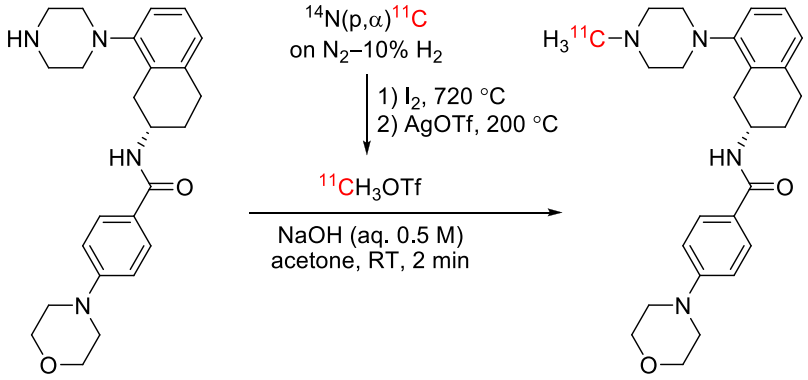

Scheme 2. Radiolabeling of [^{11}C]AZ11895987.

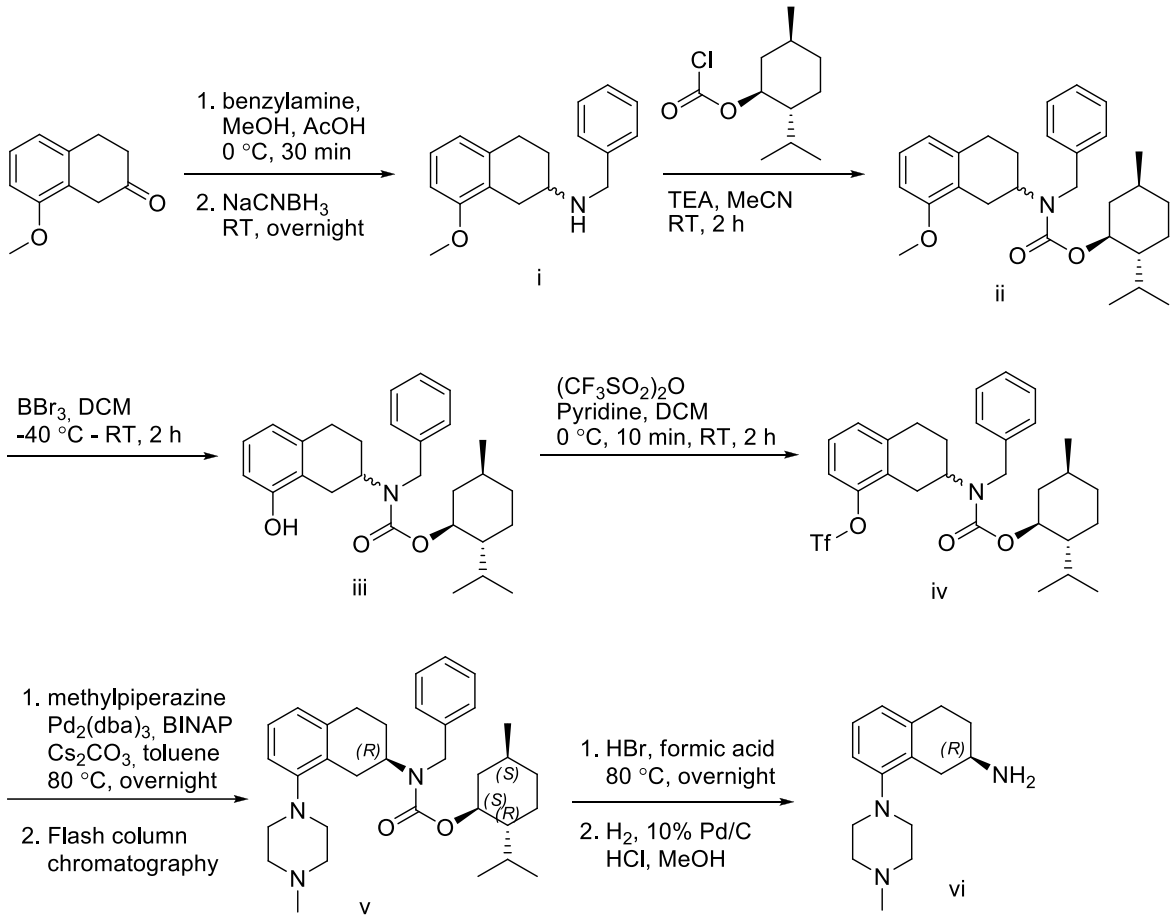

Scheme 3. Synthesis of (*R*)-8-(4-methylpiperazin-1-yl)-1,2,3,4-tetrahydronaphthalen-2-amine. Isolated yields for each of the intermediates, i) 85% ii) 92% iii) 83% iv) 68% v) 81% vi) 90%.

[^{11}C]AZ11136118. AZ11136118 was unstable in the demethylation reaction described in *paper I* and was synthesized from commercial starting material (**Scheme 3**). A multi-step synthesis was designed and performed in good overall yields (36% over 6 steps) to give enantiomerically pure (*R*)-8-(4-methylpiperazin-1-yl)-1,2,3,4-tetrahydronaphthalen-2-amine. Starting from 8-methoxy-2-tetralone, the first step was a reductive amination with benzylamine followed by addition of (*R*)-menthyl group both as protection and as a chiral derivatization agent. The methoxy-group was made into a more reactive LG by demethylation followed by reaction with

triflate anhydride. The triflate was replaced by methyl-piperazine in a Buchwald-Hartwig amination. At this point the diastereomers could be derivatized by flash column chromatography. Both diastereomers were deprotected in two steps and their respective optical rotations were compared with a sample of enatiomerically pure (*R*)-8-(4-methylpiperazin-1-yl)-1,2,3,4-tetrahydronaphthalen-2-amine provided by AstraZeneca.

4-Iodophenyl methanesulfonate was synthesized in one step from 4-iodophenol in quantitative yields (**Scheme 4**).

Radiolabelling of [^{11}C]AZ11136118 was optimized in a 2-step synthesis using [^{11}C]CO in a pressurized loop with 4-Iodophenyl methanesulfonate, Pd_2dba_3 and Xantphos in THF (**Scheme 4**). This mixture was pumped into a second vessel containing (*R*)-8-(4-methylpiperazin-1-yl)-1,2,3,4-tetrahydronaphthalen-2-amine in THF with trace amount of TBA. Subsequent purification by preparative HPLC and formulation in sterile saline yielded [^{11}C]AZ11136118 in sufficient amounts (1240 ± 347 MBq), A_m (83 ± 51 GBq/ µmol) and purity (>95%) for use in PET measurements in NHP and rodent.

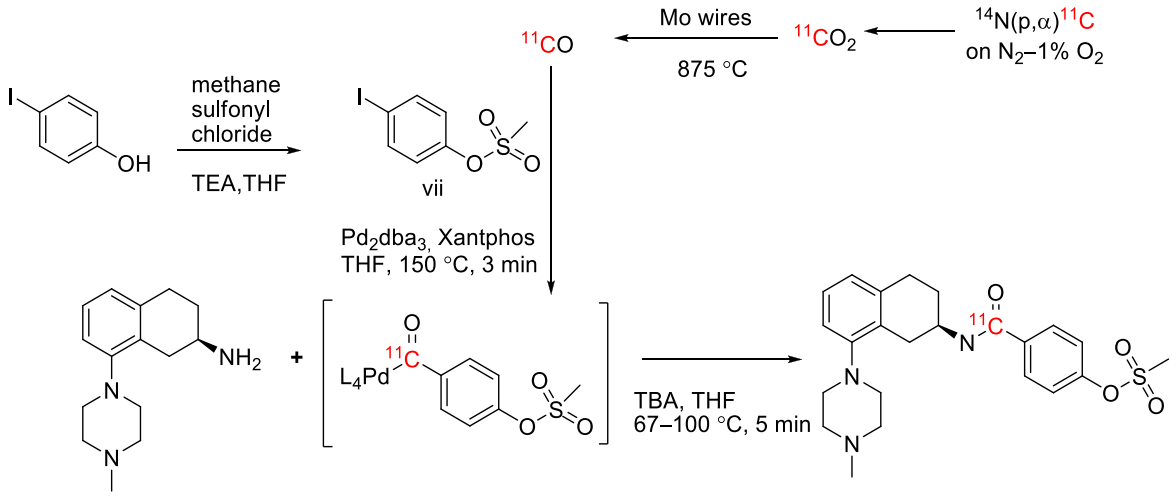

Scheme 4. Synthesis of 4-iodophenyl methanesulfonate (100% yield) and subsequent radiolabeling of [^{11}C]AZ11136118.

4.2.2 PET measurements and radioligand evaluation

PET experiments in NHP. [^{11}C]AZ11895987 and [^{11}C]AZ11136118 were used in a baseline PET measurement and showed low brain uptake with no heterogeneous regional distribution detected. [^{11}C]AZ11136118 was further investigated in NHP by blocking the efflux transporter P-gp in the BBB using tariquidar (8.0 mg/kg), which increased the brain uptake from 0.1 *SUV* to 0.4 *SUV*. Still no heterogeneous distribution in brain could be detected. In an additional PET measurement using both tariquidar (8.0 mg/kg) and A-RA000002 (2.0 mg/kg) no blocking of any specific binding could be detected. The plasma free fraction for [^{11}C]AZ11136118 and [^{11}C]AZ11895987 was 18.0 ± 0.8% (n = 3) and 50.30 ± 0.03% (n = 6) respectively.

PET experiments in rodents. [^{11}C]AZ11136118 was further investigated in rat but no 5-HT$_{1B}$ receptor specific binding could be detected in rats treated with tariquidar (8.0 mg/kg), and AR-A000002 (2.0 mg/kg). Ex-vivo PET measurements with rats and mice showed >95% of radioactivity present in brain was parent compound.

Conformational calculations The apparent pK_a of [^{11}C]AZ11136118 was measured to be 8.00 ± 0.03 (n = 3) and log$D_{7.4}$ was 2.01 ± 0.01 (n = 6) indicating that the molecule will be protonated at physiological pH. Computational calculation were made to determine the most likely structural conformation of both [^{11}C]AZ11136118 and [^{11}C]AZ11895987 along with previous successful 5-HT$_{1B}$ PET radioligands. These showed that unlike [^{11}C]AZ10419096, [^{11}C]AZ10419369 and [^{11}C]P943, both agonists are unlikely to form an intramolecular H-bond between the piperazinyl-N and the amide through a water molecule. The data from these calculations show that without this H-bond the dipolar moment is higher because it localizes the formal charge of the compound to the piperazinyl-N and hinders passive BBB diffusion (**Table 2**). Table 2 shows that the H-bonding conformations having the lowest dipole moment for each compound. But for [^{11}C]AZ11136118 and [^{11}C]AZ11895987 it also increases the ΔG and reduces the conformational stability. The BBB-penetrant radioligands all have a dipole moment below 24 Debye in their energetically favorable conformation.

Table 2. Energetics and dipole moment of the conformers of the published 5-HT$_{1B}$ PET radioligands. Conformers were obtained as described in section 3.3. Conformation **a** and **b** refers to open conformations and **c** refers to the H-bonding conformation.

Conformer	**Enthalpy (Δ*H*)** (kcal/mol)	**Gibbs free energy (Δ*G*)** (kcal/mol)	**Dipole moment** (Debye)
AZ10419369a	0	0	30.9
AZ10419369b	2.1	2.3	24.4
AZ10419369c	-1.6	-1.2	18.0
P943a	0	0	22.5
P943b	−2.3	−0.9	15.5
AZ10419096a	0	0	32.1
AZ10419096b	2.9	3.4	25.1
AZ10419096c	−2.0	−1.2	20.3
AZ11136118a	0	0	24.1
AZ11136118b	0.7	3.6	18.0
AZ11136118c	−1.0	1.8	16.3
AZ11895987a	0	0	30.9
AZ11895987b	−0.2	1.8	14.4
AZ11895987c	−1.8	0.2	12.6

4.2.3 Discussion

The project at AstraZeneca, from which the data set used to select the candidate came from, was focused on finding an antagonist which meant that very few high affinity full agonist compound were available and limited the study to just two compounds. The low brain uptake and poor regional distribution of [^{11}C]AZ11895987 was not fully investigated and the more rigorous investigation into the poor results of [^{11}C]AZ11136118 gave no clear reason for the agonists poor performance. While blocking the P-gp efflux pump increased the brain uptake, no regional distribution indicative of specific binding could be seen. The postulated possible *H*-bond in BBB penetrant 5-HT$_{1B}$ PET radioligand needed further investigation to be conclusive. PET measurements in rodent were able to determine that no radiometabolites were entering the brain.

4.3 INTRINSIC ACTIVITY IN 5-HT$_{1B}$ PET RADIOLIGANDS (*PAPER III*)

A summary of the results from *paper III*.

[^{11}C]AZ10419096, [^{11}C]AZ12175002 and [^{11}C]AZ10419369, three high-affinity ^{11}C-labeled 5-HT$_{1B}$ PET radioligands with differing intrinsic activity were used in PET measurements in monkey to evaluate their sensitivity to fenfluramine induced changes in endogenous 5-HT concentrations.

4.3.1 Radiochemistry

[^{11}C]AZ12175002 and [^{11}C]AZ10419096 were both labelled through the ^{11}C-methylation procedure described in section **3.1.2** in sufficient amounts (1946 ± 704 MBq and 1125 ± 360 MBq respectively), A_m (974 ± 636 GBq/µmol and 639 ± 205 GBq/µmol respectively) and with high radiochemical purity (>97%) for use in PET measurements in NHP.

4.3.2 PET measurements

One monkey was used in a baseline PET measurement using [^{11}C]AZ12175002 followed 2.5 hours later by a pretreatment PET measurement using AR-A000002 (2.0 mg/kg) given 30 min prior to injection of radioligand. Binding of [^{11}C]AZ12175002 was blocked by 90% in occipital cortex showing high specific binding to 5-HT$_{1B}$ receptors.

Two monkeys were used in baseline PET measurements followed three hours later by a displacement PET experiment using fenfluramine (1.0 and 5.0 mg/kg) given 15 min after injection of radioligand. Changes in regional BP_{ND} for occipital cortex between 45 and 123 min were calculated using SRTM. At the higher dose of fenfluramine the relative displacement of radioligand increased with increased agonistic efficacy (**Figure 11**). The agonistic [^{11}C]AZ12175002 showed a decrease in BP_{ND} of 60% compared to 52% for [^{11}C]AZ10419369 and 40% for the full antagonist [^{11}C]AZ10419096.(112, 125) At the lower dose of fenfluramine this correlation was not evident. At this dose, the antagonistic [^{11}C]AZ10419096 shows the

lowest decrease (19%) but the agonistic [^{11}C]AZ12175002 only slightly higher (21%) and the mixed efficacy [^{11}C]AZ10419369 the highest (30%). All three radioligands showed dose dependent displacement.

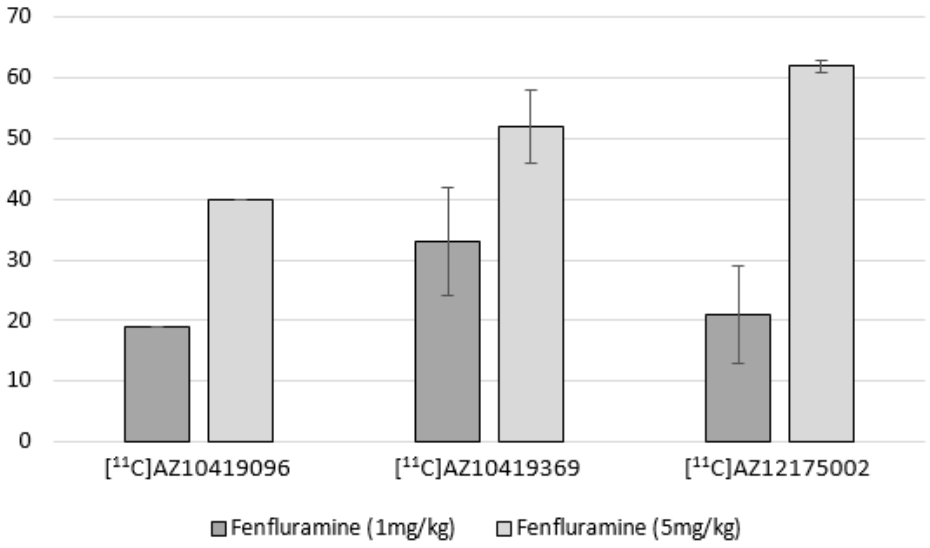

Figure 11. Displacement of radioligand by endogenous 5-HT in percent using fenfluramine (1.0 mg/kg and 5.0 mg/kg). Results for [^{11}C]AZ10419096 at fenfluramine (5.0 mg/kg) are based on one monkey (125). Results for [^{11}C]AZ10419369 at both doses are based on three monkeys (112). All other results are based on 2 monkeys.

The BP_{ND} (45−123 min) calculated for the three radioligands also increases with increasing antagonistic efficacy from 0.9 for the agonistic [^{11}C]AZ12175002 and 1.9 for [^{11}C]AZ10419369 to 3.2 for the antagonistic [^{11}C]AZ10419096. A higher uptake in cerebellum for [^{11}C]AZ12175002 could also be detected.

4.3.3 Discussion

The evaluation of how intrinsic efficacy in a 5-HT$_{1B}$ PET radioligands affects its sensitivity towards competition from endogenous 5-HT was hampered by the lack of a full agonist radioligand (see section **4.2**). Instead, [^{11}C]AZ12175002 was used, a highly agonistic compound with some antagonist effect (110). The results were not enough to conclusively uphold or dismiss the theory that an agonist PET radioligand would be displaced to a higher extent by endogenous 5-HT competition than an antagonist. But considering the challenges in undertaking such a PET study, the results establish some parameters for future extended studies. Three structurally similar high affinity 5-HT$_{1B}$ PET radioligands were developed, with differing intrinsic activity. All three displayed a dose-dependent sensitivity towards fenfluramine induced changes in synaptic 5-HT concentrations. A dose range of fenfluramine was established within which an extended study can take place. The problem of comparing data from different individuals was apparent and should be avoided, instead multiple PET measurements in each individual are desired. Another trend is also evident; the BP_{ND} increases with increasing antagonist activity. This follows the idea that an antagonist would have a higher concentration of available receptors to bind to than an agonist, as an antagonist can bind

indiscriminately to all affinity states of the receptor. Any exact quantification of this is not feasible as several unknown parameters are involved. A problem in visualizing the high and low affinity state of GPRCs *in vivo* is the difficulty in developing agonist PET radioligands because the affinity measured in *in vitro* assays may not accurately capture the true affinity and selectivity in a dynamic system in presence of several subtypes of the receptor (126). As an agonist tends to have a closer structural similarity to the endogenous ligand, off-target binding is an increasing risk for agonist PET radioligands for 5-HT receptors, as there are several 5-HT receptor subtypes with whom endogenous 5-HT interacts. It is also unclear if the distinct difference between high and low affinity seen *in vitro* can be replicated *in vivo* where a receptor could potentially be involved in several conformations within the duration of a PET measurement (127, 128).

4.4 FLUORINE-18 5-HT$_{1B}$ PET RADIOLIGAND (*PAPER IV*)

A summary of the results from *paper IV*.

[^{18}F]AZ10419096 is structurally identical to [^{11}C]AZ10419096 only differing in type of radionuclide used. The structure of AZ10419096 contains two fluorine substituents either of which might be exchanged potentially with fluorine-18. The choice of fluorine to exchange was directed by the availability of starting material from AstraZeneca.

4.4.1 Chemistry and radiochemistry

The available chloro-analog of AZ10419096 was used to synthesize the boronate precursor in good yield (91%). The precursor is susceptible to de-borylation in protic solvents and could not be purified with chromatographical techniques, but instead had to be isolated by a simplified crystallization method. This meant the purity of the precursor could not be accurately measured by HPLC. Radio-fluorination was performed using copper-catalyzed fluorination of the borate, a recently developed methodology (129). The radiofluorination reaction only gave low *RCY* (<5%), perhaps linked to the instability of the precursor, but was able to produce sufficient amounts (350 MBq) of high radiochemical purity (> 97%) and A_m (150 GBq/µmol) for use in PET measurements in NHP.

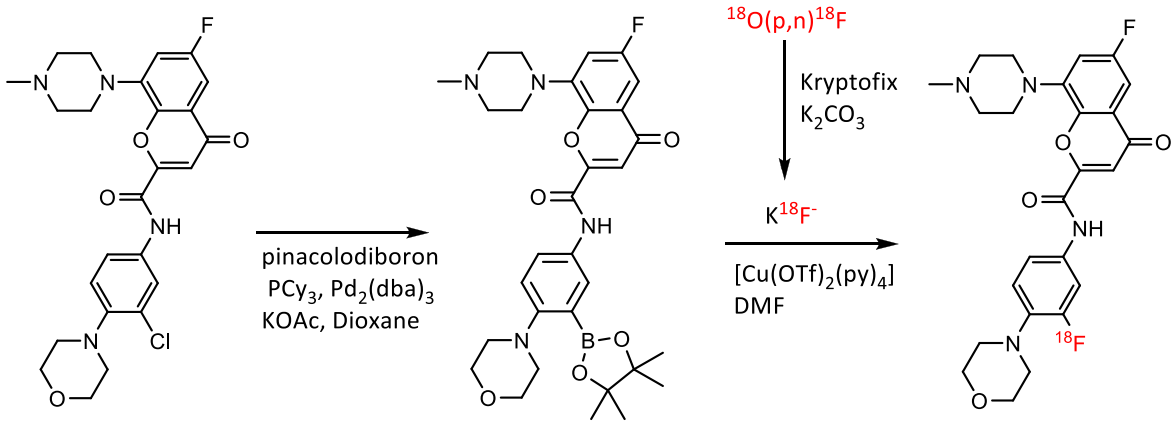

Scheme 5. Synthesis scheme of precursor and radiolabeling of [^{18}F]AZ10419096.

4.4.2 PET measurements

A baseline PET measurement using [^{18}F]AZ10419096 showed brain uptake and regional distribution consisted with the structurally identical [^{11}C]AZ10419096 (**Figure 12** and **13A**). The ratio of radioactivity in ROIs to cerebellum peaked within 60 min and remained at that level thereafter (**Figure 13B**). BP_{ND} was calculated using SRTM with cerebellum as reference region to be 1.37 for occipital cortex and 1.54 globus pallidus. In pretreatment PET measurement using AR-A000002 (2.0 mg/kg) administered 30 min prior to [^{18}F]AZ10419096, binding was blocked by 80% in occipital cortex and 70% in whole brain showing high specific binding to 5-HT$_{1B}$ receptors in brain (**Figure 12** and **13C**).

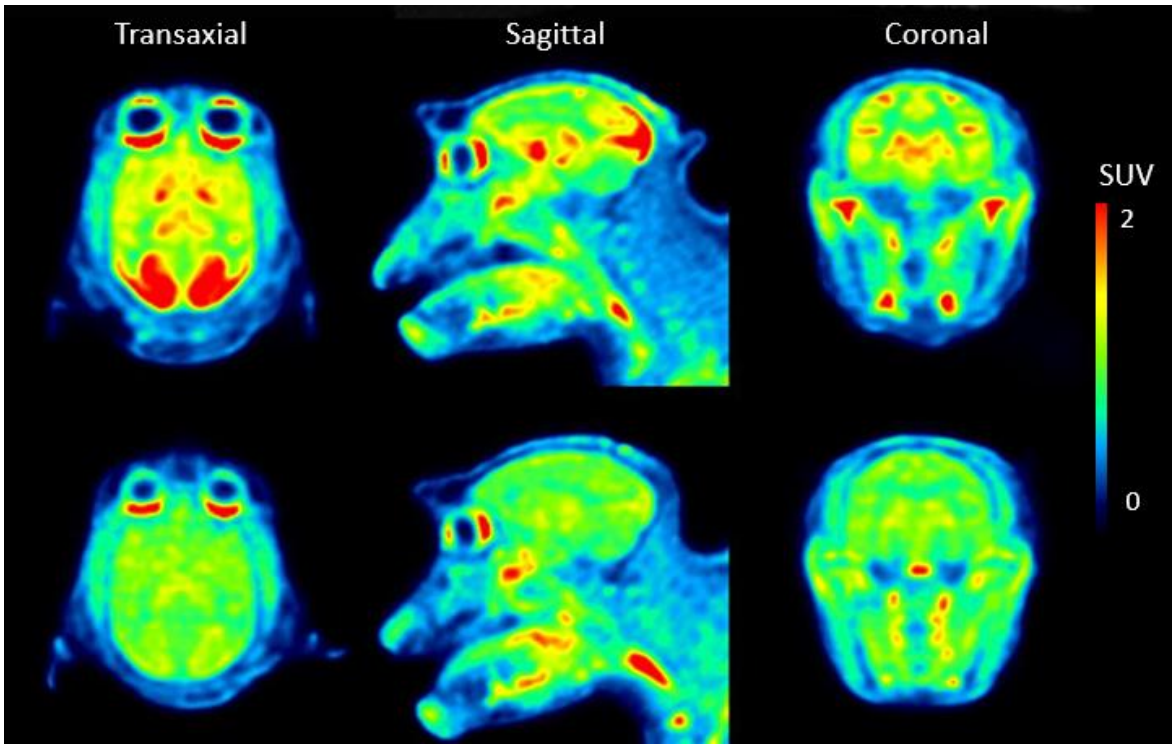

Figure 12. PET summation images (0−123 min); Top row; PET summation images from baseline PET measurement using [^{18}F]AZ10419096; Bottom row; PET summation images from PET measurement with AR-A000002 (2.0 mg/kg) given 30 min before [^{18}F]AZ10419096.

Radiometabolite analysis of plasma sampled during PET measurements showed at 60 min after administration, parent radioligand represented ~ 50% of radioactivity in plasma (**Figure 10**). The percentage of radioligand free in plasma was ~30%.

4.4.3 Discussion

[^{18}F]AZ10419096 is the first fluorine-18 PET radioligand for imaging 5-HT$_{1B}$ receptors in brain. It shows favorable pharmacological properties and could be a useful tool in further research of serotonergic system. The chemistry needs improvement as both precursor synthesis and radiofluorination methodology met with challenges. The stability of the borate precursor was low which most likely led to the radiofluorination only working in low radiochemical yields.

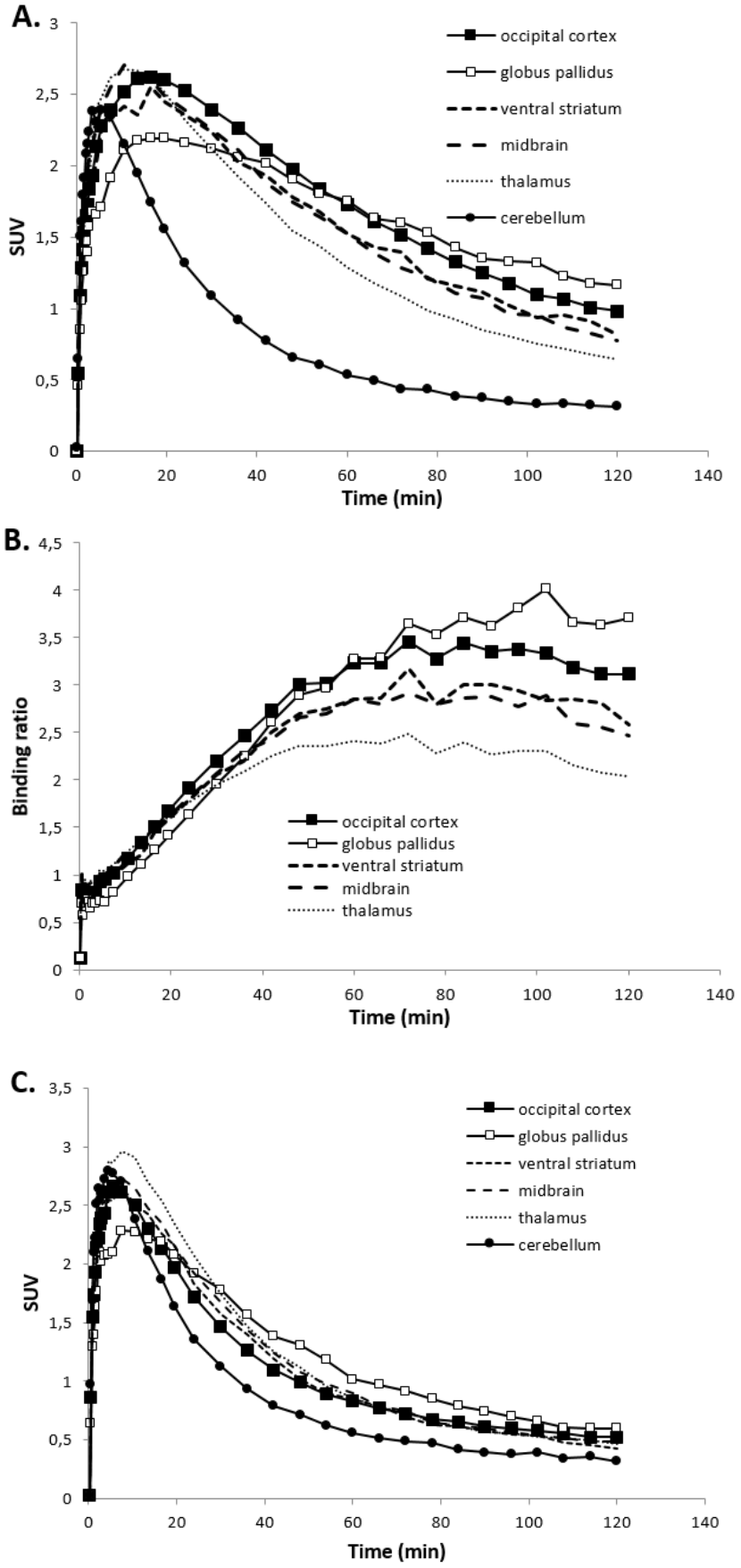

Figure 13. A. Regional time-activity curves from baseline PET measurement (SUV, 0-123 min) using [^{18}F]AZ10419096. **B**. Regional binding ratio from baseline PET measurement using [^{18}F]AZ10419096. **C**. Regional time-activity curves from pretreatment PET measurement using [^{18}F]AZ10419096, AR-A000002 (2.0 mg/kg) was given 30 min before the radioligand.

4.5 ADDITIONAL COMMENTS AND DISCUSSION

Some additional comments and discussion points not directly linked to one specific paper.

4.5.1 Chemistry

^{11}C-*N*-methylation using [^{11}C]CH_3OTf was successfully used to produce [^{11}C]AZ10419096 as well as [^{11}C]AZ11895987 and [^{11}C]AZ12175002 in sufficient yields and A_m and with high radiochemical purity. The desmethyl precursor for [^{11}C]AZ10419096 used in *paper I* could be synthesized from a reference sample in high purity but in low yields. This approach was also attempted with AZ11136118 and a few other non-published compounds. However, the demethylation reaction using 2-chloroethyl chloroformate in most cases gave high amounts of by-product and little-to-no desired product. A more consistently successful approach, albeit more time-consuming, proved to be to synthesize the desmethyl-precursor from simpler starting material using a protected piperazinyl group, as was the case for both [^{11}C]AZ10419096 and [^{11}C]AZ12175002 used in *paper III*.

4.5.2 Agonist 5-HT$_{1B}$ PET radioligands

In his thesis, no full agonist was successfully developed as a useful 5-HT$_{1B}$ PET radioligand. Whether a full agonist can be developed remains to be seen, as the full agonists [^{11}C]AZ11136118 and [^{11}C]AZ11895987 failed to enter the brain in any useful amounts even with efflux transporter P-gp blocked. A highly agonistic PET radioligand previously identified was further characterized, [^{11}C]AZ12175002. [^{11}C]AZ11895987 and [^{11}C]AZ12175002 have close structural similarities, only differing in the direction and stereochemistry of the central amide as well as the oxygen in bicyclic ring system (**Figure 7**). They also share a strong structural similarity with AR-A000002, which is used in this thesis to block the 5-HT$_{1B}$ receptors in brain and therefore is able to pass through the BBB, in higher doses than a PET micro-dose at least.

In *paper II*, a proposed reason for the poor brain uptake was the inability of [^{11}C]AZ11136118 and [^{11}C]AZ11895987 to form an energetically favorable *H*-bond between the protonated piperazinyl nitrogen and the amide, aided by a water molecule. This *H*-bond lowers the dipole moment of the molecule and attenuates the formal charge of the protonated methyl-piperazine. According to additional quantum calculations performed later for this thesis, [^{11}C]AZ12175002 seem equally unlikely to form a *H*-bond as [^{11}C]AZ11895987 as evidenced by the higher free energy (ΔG) of the *H*-bond conformation **c** (**Table 3**). AR-A000002 also seem unlikely to form an *H*-bond but has never been used in a micro-dose so its brain uptake might be low but enough to have effect in a higher dose. The comparatively similar results for non-BBB-penetrant [^{11}C]AZ11895987 and BBB-penetrant [^{11}C]AZ12175002 shows that this explanation is overly simplistic and that other factors must also be considered. Firstly, as a basis for this idea was the measured apparent pK_a of [^{11}C]AZ11136118 and it was assumed that all methyl-piperazinyl groups would have similar pK_a values around 8.0. With a lower pK_a value the need for attenuating a formal charge would not be needed as the piperazinyl-*N* would not be protonated. Secondly, the calculations only considers one intramolecular interaction and potentially there

could be other interactions to consider. Thirdly, the poor brain uptake for full agonists could be due to other issues entirely, such as lack of binding to 5-HT_{1B} receptors and/or active transport out of the brain by efflux transporter other than P-gp. One such possibility is that an agonist with high affinity to a 5-HT receptor would potentially also be a substrate for 5-HTT mediated transport inside the neuron and subsequently out from brain. 5-HTTs expression along the axons would also prevent the radioligand from ever reaching the 5-HT_{1B} receptors in the synapse.(130)

Table 3. Quantum calculations of AR-A000002 and [^{11}C]AZ12175002 compared with structurally similar [^{11}C]AZ11895987. Conformation **a** and **b** refers to open conformations and **c** refers to the *H*-bonding conformation.

Conformer	**Enthalpy (Δ*H*)** (kcal/mol)	**Gibbs free energy (Δ*G*)** (kcal/mol)	**Dipole moment** (Debye)
AR-A000002a	0	0	29.4
AR-A000002b	−1.7	1.1	12.1
AR-A000002c	0.1	2.6	14.1
AZ12175002a	0	0	25.4
AZ12175002b	1.3	2.2	17.0
AZ12175002c	−1.6	0.2	12.5
AZ11895987a	0	0	30.9
AZ11895987b	−0.2	1.8	14.4
AZ11895987c	−1.8	0.2	12.6

5 SUMMARY OF FINDINGS

The overall focus within this thesis has been to develop 5-HT_{1B} PET radioligands to image 5-HT_{1B} receptors in brain. In total three novel carbon-11 PET radioligands were developed, [^{11}C]AZ10419096, [^{11}C]AZ11136118, [^{11}C]AZ11895987; one carbon-11 PET radioligand which previously had been published was further investigated, [^{11}C]AZ12175002; and one fluorine-18 PET radioligand was developed, [^{18}F]AZ10419096 (**Figure 14**).

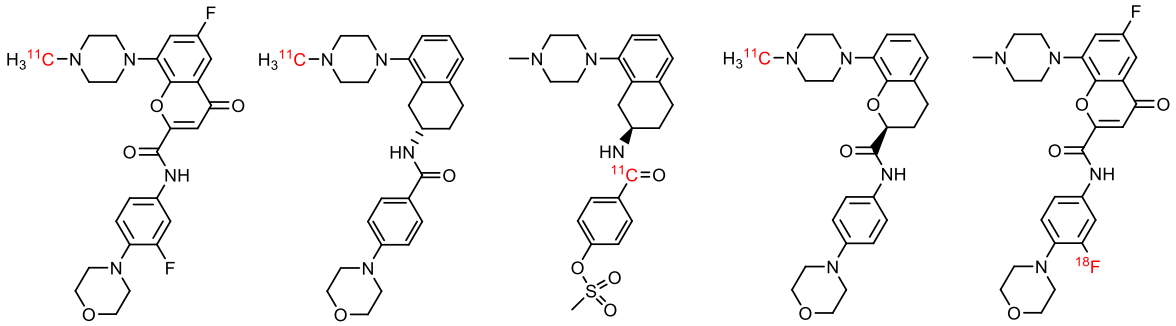

[^{11}C]AZ10419096 ***paper I & III*** | **[^{11}C]AZ11895987** ***paper II*** | **[^{11}C]AZ11136118** ***paper II*** | **[^{11}C]AZ12175002** ***paper III*** | **[^{18}F]AZ10419096** ***paper IV***

Figure 14. The 5-HT_{1B} PET radioligands that have been developed as part of this thesis.

In *paper I*, [^{11}C]AZ10419096: a full antagonist 5-HT_{1B} PET radioligand labelled with carbon-11 was developed. [^{11}C]AZ10419096 showed high specific binding in pretreatment PET measurements and was displaced by fenfluramine-induced increase in 5-HT concentrations in a dose-dependent manner.

In *paper II*, no full agonist PET radioligand was developed. Two full agonists were identified but neither was useful as a PET radioligand. The high-affinity agonists were labelled with carbon-11 and both showed poor brain uptake and no specific binding could be detected in PET measurements. No clear reason could be determined for the poor performance of the agonist PET radioligands.

In *paper III*, a highly agonistic, previously published compound was further developed and characterized, [^{11}C]AZ12175002, and could be used in an initial pilot study comparing three PET radioligands, [^{11}C]AZ10419096, [^{11}C]AZ10419369 and [^{11}C]AZ12175002, with differing intrinsic activity. Displacement PET measurements comparing two different doses of fenfluramine were performed and resulted in useful guidelines for a future larger study in imaging the different affinity states of the 5-HT_{1B} receptor.

In *paper IV*, a fluorine-18 labelled 5-HT_{1B} PET radioligand, [^{18}F]AZ10419096, that is the identical structure of [^{11}C]AZ10419096 was developed and showed high specific binding in pretreatment PET measurements. This is the first promising fluorine-18 labelled 5-HT_{1B} PET radioligand but will require further development before it can be used in any larger PET study.

6 FUTURE CONSIDERATIONS AND CHALLENGES

Development of agonist CNS PET radioligands. The disappointing results in developing a full agonist 5-HT_{1B} PET radioligand does not mean it is impossible to do so. Future projects with this aim will need to find new candidate compounds, which would mean setting up *in vitro* assays to determine affinity and efficacy. The candidate compounds could be structurally similar to the failed agonists developed herein and one idea would be to reverse the amide bond of the two full agonist tested, [^{11}C]AZ11136118 and [^{11}C]AZ11895987, or incorporate a hetero-atom in the bicyclic ring.

A pretreatment PET measurement using either [^{11}C]AZ11136118 or [^{11}C]AZ11895987 with a SSRI as blocking agent would answer the speculation of whether 5-HTT transportation of the radioligands is the reason for the poor binding and poor brain uptake for both full agonists.

Intrinsic activity evaluation. A complete study into agonist/antagonist relative ability to measure changes in endogenous 5-HT concentration could be performed. A recommendation for how such a study should be designed was outlined in *paper III*. Three PET radioligand with differing intrinsic activity were identified with dose dependent displacement by fenfluramine-induced changes in endogenous 5-HT concentrations.

[^{18}F]AZ10419096. The first fluorine-18 labelled PET radioligand for imaging 5-HT_{1B} receptors in brain show good characteristics for further development. Some issues remain to be resolved before that can take place.

A reliable synthesis route for the precursor needs to be established, subsequent attempts at precursor synthesis by an external contractors has failed. If a reliable synthesis route cannot be established for this precursor, a different overall approach needs to be developed using different precursor and different radiofluorination methodology. A precursor for radiofluorination on the other fluorine-site of the AZ10419096 molecule would be the obvious first option (**Figure 7**). If the boronic ester precursor to [^{18}F]AZ10419096 can be reliably synthesized, optimization to the radiofluorination would be needed. Reducing the amount of precursor needed per synthesis is key for further development. Developing the existing radiofluorination methodology on a micro-fluidic system could reduce the amount of precursor and solvent in the reaction mixture while maintaining the stoichiometric ratios.

7 ACKNOWLEDGEMENTS

This thesis was made possible as part of the Karolinska Institutet/NIH doctoral program. I would like to extend my sincere gratitude and thanks to everyone who has made this thesis possible.

Professor Christer Halldin, my main supervisor, for giving me the opportunity and pleasure of doing my doctoral training at Karolinska Institutet, for teaching me about PET chemistry and imaging and showing me how to become an independent researcher in the future.

Dr. Victor W. Pike, my NIH/NIMH supervisor, for the opportunity and pleasure of working in his research group at NIMH and for sharing his vast experience and knowledge of scientific research in general and PET radiochemistry in particular.

Dr. Magnus Schou and Dr. Sangram Nag, my co-supervisors at Karolinska Institutet, for their instructive and continuous assistance and for their great friendship and support.

Dr. Chad Elmore, my co-supervisor at AstraZeneca, for lending me the use of his lab and his expertise and for his critical analytical input. I also want to thank Dr. Cecilia Ericsson at AstraZeneca for her assistance during my brief stay there.

I want to thank all current and previous members of the KI PET group:

Professor Lars Farde, Professor Balázs Gulyás, associate professor Andrea Varrone,Arsalan Amir, Gennaudi Jogolev, Dr. Maria Johansson, Dr. Mohammad Madhi Moein, Dr. Nahid Amini, Madjid Ebrahimi-Mehrabani, Youssef El-Khoury, Dr. Kenneth Dahl, Dr. Peter Johnström, Dr. Zhisheng Jia, Dr. Vladimir Stepanov, Johan Ulin, Prodip Datta, Dr. Mikhail Kondrashov, Dr. Patricia Miranda Azpiazu, Karin Zahir, Åsa Södergren, Siv Eriksson, Kaisa Horrka, Mélodie Ferrat, Dr. Ana Vazquez Romero, Dr. Arindam Das, Dr. Mahabuba Jahan, Henrik Alfredéen, Göran Rosenqvist, Nadja Hellsing, Jonas Ahlgren, Dr. Akihiro Takano, Dr. Ryosuke Arakawa, Dr. Kai-Chun Yang, Junya Matsumoto, Tsuyoshi Nogami, Dr. Marie Svedberg, Urban Hansson, Nina Knave, Malena Kjellén, Opokua Britton Cavaco, Dr. Per Stenkrona, Dr. Mikael Tiger, Dr. Martin Schain, Dr. Katarina Varnäs, Dr. Jacqueline Borg, Dr. Simon Cervenka, Dr. Magdalena Nord, Dr. Karin Collste, Dr. Patrik Fazio, Dr. Johan Lundberg, Dr. Granville Matheson, Dr. Pontus Plavén-Sigray, Dr. Anton Forsberg, Dr. Miklós Tóth, Dr. Jenny Häggkvist, Lenke Tari, Sara Lundqvist, Susanna Nevala, Zsolt Sarnyai Dr. Jonas Malmqvist and Dr. Evegeni Revunov. Thank you for all the help and support during the four years.

All current and previous members of the Karolinska QA group:

Hanna Elgstrand, Anne Byström, Carsten Steiger and Emma Meyer.

I also want to thank all the members of the Molecular imaging branch at NIMH:

Dr. Shuiyu Lu, Dr. Stefano Altomonte, Dr. Sanjay Telu, Dr. Fabrice Simeon, Cheryl Morse, Dr. Umesha Shetty, Dr. Sami S. Zoghbi, Dr. Jinsoo Hong, Dr. Yong Lee Sook, Dr. Bo Yuen Yang, Dr. Lisheng Cai, William Miller and Elizabeth Alzona as well as Dr. Robert Innis for making my stay at NIMH and Bethesda a pleasurable experience

Finally, I would like to thank my wife, my family and my friends for all their love and support.

8 REFERENCES

1. Halldin C, Gulyas B, Langer O, Farde L. Brain radioligands - State of the art and new trends. Quarterly Journal of Nuclear Medicine. 2001;45(2):139-52.

2. Halldin C, Gulyas B, Farde L. PET studies with carbon-11 radioligands in neuropsychopharmacological drug development. Current Pharmaceutical Design. 2001;7(18):1907-29.

3. Phelps ME. Positron emission tomography provides molecular imaging of biological processes. Proceedings of the National Academy of Sciences of the United States of America. 2000;97(16):9226-33.

4. Lee CM, Farde L. Using positron emission tomography to facilitate CNS drug development. Trends in Pharmacological Sciences. 2006;27(6):310-6.

5. Matthews PM, Rabiner EA, Passchier J, Gunn RN. Positron emission tomography molecular imaging for drug development. British Journal of Clinical Pharmacology. 2012;73(2):175-86.

6. Bergstrom M, Grahnen A, Langstrom B. Positron emission tomography microdosing: a new concept with application in tracer and early clinical drug development. European Journal of Clinical Pharmacology. 2003;59(5-6):357-66.

7. Verbruggen A, Coenen HH, Deverre J-R, Guilloteau D, Langstrom B, Salvadori PA, et al. Guideline to regulations for radiopharmaceuticals in early phase clinical trials in the EU. European Journal of Nuclear Medicine and Molecular Imaging. 2008;35(11):2144-51.

8. Wagner HN, Burns HD, Dannals RF, Wong DF, Langstrom B, Duelfer T, et al. Imaging dopamine-receptors in the human-brain by positron emission tomography. Science. 1983;221(4617):1264-6.

9. Gomez-Vallejo V, Gaja V, Gona KB, Llop J. Nitrogen-13: historical review and future perspectives. Journal of Labelled Compounds & Radiopharmaceuticals. 2014;57(4):244-54.

10. Miller PW, Long NJ, Vilar R, Gee AD. Synthesis of ^{11}C, ^{18}F, ^{15}O, and ^{13}N Radiolabels for Positron Emission Tomography. Angewandte Chemie-International Edition. 2008;47(47):8998-9033.

11. Eriksson L, Dahlbom M, Widen L. Positron emission tomography - A new technique for studies of the central nervous system. Journal of Microscopy-Oxford. 1990;157:305-33.

12. Cherry SR. Fundamentals of positron emission tomography and applications in preclinical drug development. Journal of Clinical Pharmacology. 2001;41(5):482-91.

13. Huang SC, Barrio JR, Yu DC, Chen B, Grafton S, Melega WP, et al. Modeling approach for separating blood time-activity curves in positron emission tomographic studies. Physics in Medicine and Biology. 1991;36(6):749-61.

14. Zhang Y, Fox GB. PET imaging for receptor occupancy: meditations on calculation and simplification. Journal of biomedical research. 2012;26(2):69-76.

15. Lipinski CA, Lombardo F, Dominy BW, Feeney PJ. Experimental and computational approaches to estimate solubility and permeability in drug discovery and development settings. Advanced Drug Delivery Reviews. 1997;23(1-3):3-25.

16. Zhang MQ, Wilkinson B. Drug discovery beyond the 'rule-of-five'. Current Opinion in Biotechnology. 2007;18(6):478-88.

17. Meanwell NA. Improving Drug Candidates by Design: A Focus on Physicochemical Properties As a Means of Improving Compound Disposition and Safety. Chemical Research in Toxicology. 2011;24(9):1420-56.

18. Pike VW. Considerations in the Development of Reversibly Binding PET Radioligands for Brain Imaging. Current Medicinal Chemistry. 2016;23(18):1818-69.

19. Pike VW. PET radiotracers: crossing the blood-brain barrier and surviving metabolism. Trends in Pharmacological Sciences. 2009;30(8):431-40.

20. Innis RB, Cunningham VJ, Delforge J, Fujita M, Giedde A, Gunn RN, et al. Consensus nomenclature for in vivo imaging of reversibly binding radioligands. Journal of Cerebral Blood Flow and Metabolism. 2007;27(9):1533-9.

21. Laruelle M, Slifstein M, Huang YY. Positron emission tomography: imaging and neurotransporter availability. Methods. 2002;27(3):287-99.

22. Demeule M, Regina A, Jodoin J, Laplante A, Dagenais C, Berthelet F, et al. Drug transport to the brain: Key roles for the efflux pump P-glycoprotein in the blood-brain barrier. Vascular Pharmacology. 2002;38(6):339-48.

23. Begley DJ. ABC transporters and the blood-brain barrier. Current Pharmaceutical Design. 2004;10(12):1295-312.

24. Amini N, Nakao R, Schou M, Halldin C. Identification of PET radiometabolites by cytochrome P450, UHPLC/Q-ToF-MS and fast radio-LC: applied to the PET radioligands [^{11}C]flumazenil, [^{18}F]FE-PE2I, and [^{11}C]PBR28. Analytical and Bioanalytical Chemistry. 2013;405(4):1303-10.

25. Ma Y, Kiesewetter DO, Lang LX, Gu DY, Chen XY. Applications of LC-MS in PET Radioligand Development and Metabolic Elucidation. Current Drug Metabolism. 2010;11(6):483-93.

26. Amini N, Nakao R, Schou M, Halldin C. Determination of plasma protein binding of positron emission tomography radioligands by high-performance frontal analysis. Journal of Pharmaceutical and Biomedical Analysis. 2014;98:140-3.

27. Coenen HH, Gee AD, Adam M, Antoni G, Cutler CS, Fujibayashi Y, et al. Consensus nomenclature rules for radiopharmaceutical chemistry - Setting the record straight. Nuclear Medicine and Biology. 2017;55:V-XI.

28. Sergeev M, Lazari M, Morgia F, Collins J, Javed MR, Sergeeva O, et al. Performing radiosynthesis in microvolumes to maximize molar activity of tracers for positron emission tomography. Communications Chemistry. 2018;1.

29. Shields AF, Graham MM, Kozawa SM, Kozell LB, Link JM, Swenson ER, et al. Contribution of labeled carbon-dioxide to PET imaging of carbon-11-labeled compounds. Journal of Nuclear Medicine. 1992;33(4):581-4.

30. Taddei C, Gee AD. Recent progress in [^{11}C]carbon dioxide ([^{11}C]CO_2) and [^{11}C]carbon monoxide ([^{11}C]CO) chemistry. Journal of Labelled Compounds & Radiopharmaceuticals. 2018;61(3):237-51.

31. Langstom B, Itsenko O, Rahman O. [^{11}C]Carbon monoxide, a versatile and useful precursor in labelling chemistry for PET ligand development. Journal of Labelled Compounds & Radiopharmaceuticals. 2007;50(9-10):794-810.

32. Rahman O. [^{11}C]Carbon monoxide in labeling chemistry and positron emission tomography tracer development: scope and limitations. Journal of Labelled Compounds & Radiopharmaceuticals. 2015;58(3):86-98.

33. Finn RD, Christman DR, Ache HJ, Wolf AP. Preparation of [^{11}C]cyanide for use in synthesis of organic radiopharmaceuticals II. International Journal of Applied Radiation and Isotopes. 1971;22(12):735-+.

34. Sandell J, Halldin C, Hall H, Thorberg SO, Werner T, Sohn D, et al. Radiosynthesis and autoradiographic evaluation of [^{11}C]NAD-299, a radioligand for visualization of the 5-HT1A receptor. Nuclear Medicine and Biology. 1999;26(2):159-64.

35. Wilson AA, Garcia A, Houle S, Sadovski O, Vasdev N. Synthesis and Application of Isocyanates Radiolabeled with Carbon-11. Chemistry-a European Journal. 2011;17(1):259-64.

36. Larsen P, Ulin J, Dahlstrom K, Jensen M. Synthesis of [^{11}C]iodomethane by iodination of C-11 methane. Applied Radiation and Isotopes. 1997;48(2):153-7.

37. Wuest F, Berndt M, Kniess T. Carbon-11 labeling chemistry based upon [^{11}C]methyl iodide. PET Chemistry: The driving force in molecular imaging. 2007;62:183-213.

38. Jewett DM. A simple synthesis of [^{11}C]methyl triflate. Applied Radiation and Isotopes. 1992;43(11):1383-5.

39. Nagren K, Muller L, Halldin C, Swahn CG, Lehikoinen P. Improved synthesis of some commonly used PET radioligands by use of [^{11}C]methyl triflate. Nuclear Medicine and Biology. 1995;22(2):235-9.

40. Miller PW, Bender D. ^{11}C Carbon Disulfide: A Versatile Reagent for PET Radiolabelling. Chemistry-a European Journal. 2012;18(2):433-6.

41. Shibahara O, Watanabe M, Yamada S, Akehi M, Sasaki T, Akahoshi A, et al. Synthesis of C-11-Labeled RXR Partial Agonist 14(3,5,5,8,8-Pentamethyl-5,6,7,8-tetrahydronaphthalen-2-yl)aminoThenzotr iazole-5-carboxylic Acid (CBt-PMN) by Direct C-11 Carbon Dioxide Fixation via Organolithiation of Trialkyltin Precursor and PET Imaging Thereof. Journal of Medicinal Chemistry. 2017;60(16):7139-45.

42. Rotstein BH, Liang SH, Placzek MS, Hooker JM, Gee AD, Dolle F, et al.^{11}C=O bonds made easily for positron emission tomography radiopharmaceuticals. Chemical Society Reviews. 2016;45(17):4708-26.

43. Riss PJ, Lu SY, Telu S, Aigbirhio FI, Pike VW. CuI-Catalyzed ^{11}C-Carboxylation of Boronic Acid Esters: A Rapid and Convenient Entry to 11C-Labeled Carboxylic Acids, Esters, and Amides. Angewandte Chemie-International Edition. 2012;51(11):2698-702.

44. Zeisler SK, Nader M, Theobald A, Oberdorfer F. Conversion of no-carrier-added C-11 carbon dioxide to [^{11}C]carbon monoxide on molybdenum for the synthesis of C-11-labelled aromatic ketones. Applied Radiation and Isotopes. 1997;48(8):1091-5.

45. Dahl K, Itsenko O, Rahman O, Ulin J, Sjoberg CO, Sandblom P, et al. An evaluation of a high-pressure ^{11}CO carbonylation apparatus. Journal of Labelled Compounds & Radiopharmaceuticals. 2015;58(5):220-5.

46. Roeda D, Crouzel C, Dolle F. A rapid, almost quantitative conversion of [^{11}C]carbon dioxide into [^{11}C] carbon monoxide via [^{11}C]formate and [^{11}C]formyl chloride. Radiochimica Acta. 2004;92(4-6):329-32.

47. Schoenbe.A, Heck RF. Palladium-catalyzed amidation of aryl, heterocyclic, and vinylic halides. Journal of Organic Chemistry. 1974;39(23):3327-31.

48. Schoenbe.A, Bartolet.I, Heck RF. Palladium-catalyzed carboalkoxylation of aryl, benzyl, and vinylic halides. Journal of Organic Chemistry. 1974;39(23):3318-26.

49. Dahl K, Schou M, Ulin J, Sjoberg CO, Farde L, Halldin C. C-11-carbonylation reactions using gas-liquid segmented microfluidics. Rsc Advances. 2015;5(108):88886-9.

50. Miller PW, Long NJ, de Mello AJ, Vilar R, Audrain H, Bender D, et al. Rapid multiphase carbonylation reactions by using a microtube reactor: Applications in positron emission tomography C-11-radiolabeling. Angewandte Chemie-International Edition. 2007;46(16):2875-8.

51. Mock BH. Automated [^{11}C]Methyl Iodide/Triflate Production: Current State of the Art. Current Organic Chemistry. 2013;17(19):2119-26.

52. Langstrom B, Lundqvist H. Preparation of [^{11}C]methyl iodide and its use in synthesis of [^{11}C]methyl-L-methionine. International Journal of Applied Radiation and Isotopes. 1976;27(7):357-63.

53. Gallagher BM, Fowler JS, Gutterson NI, Macgregor RR, Wan CN, Wolf AP. Metabolic trapping as a principle of radiopharmaceutical design - Some factors responsible for biodistribution of [^{18}F]2-deoxy-2-fluoro-D-glucose. Journal of Nuclear Medicine. 1978;19(10):1154-61.

54. Palmer AJ, Clark JC, Goulding RW. Preparation of F-18 labeled radiopharmaceuticals. International Journal of Applied Radiation and Isotopes. 1977;28(1-2):53-65.

55. Casella V, Ido T, Wolf AP, Fowler JS, Macgregor RR, Ruth TJ. Anhydrous F-18 labeled elemental fluorine for radiopharmaceutical preparation. Journal of Nuclear Medicine. 1980;21(8):750-7.

56. Nickles RJ, Gatley SJ, Votaw JR, Kornguth ML. Production of reactive F-18. Applied Radiation and Isotopes. 1986;37(8):649-&.

57. Cai LS, Lu SY, Pike VW. Chemistry with [^{18}F]fluoride ion. European Journal of Organic Chemistry. 2008(17):2853-73.

58. Preshlock S, Tredwell M, Gouverneur V. ^{18}F-Labeling of Arenes and Heteroarenes for Applications in Positron Emission Tomography. Chemical Reviews. 2016;116(2):719-66.

59. Sood S, Firnau G, Garnett ES. Radiofluorination with Xenon difluoride - A new high-yield synthesis of [^{18}F]2-fluoro-2-deoxy-deuterium-glucose. International Journal of Applied Radiation and Isotopes. 1983;34(4):743-5.

60. Lu SY, Pike VW. Synthesis of [^{18}F]xenon difluoride as a radiolabeling reagent from F-18 fluoride ion in a micro-reactor and at production scale. Journal of Fluorine Chemistry. 2010;131(10):1032-8.

61. Teare H, Robins EG, Arstad E, Luthra SK, Gouverneur V. Synthesis and reactivity of [^{18}F]-*N*-fluorobenzenesulfonimide. Chemical Communications. 2007(23):2330-2.

62. Teare H, Robins EG, Kirjavainen A, Forsback S, Sandford G, Solin O, et al. Radiosynthesis and Evaluation of [^{18}F]Selectfluor bis(triflate). Angewandte Chemie-International Edition. 2010;49(38):6821-4.

63. Gao ZH, Lim YH, Tredwell M, Li L, Verhoog S, Hopkinson M, et al. Metal-Free Oxidative Fluorination of Phenols with [^{18}F]Fluoride. Angewandte Chemie-International Edition. 2012;51(27):6733-7.

64. Lee E, Kamlet AS, Powers DC, Neumann CN, Boursalian GB, Furuya T, et al. A Fluoride-Derived Electrophilic Late-Stage Fluorination Reagent for PET Imaging. Science. 2011;334(6056):639-42.

65. Coenen HH. Fluorine-18 labeling methods: Features and possibilities of basic reactions. PET Chemistry: The driving force in molecular imaging. 2007;62:15-50.

66. Jewett DM, Toorongian SA, Bachelor MA, Kilbourn MR. Extraction of ^{18}F-fluoride from ^{18}O-water by a fast fibrous anion exchange resin. Applied Radiation and Isotopes. 1990;41(6):583-6.

67. Coenen HH, Klatte B, Knochel A, Schuller M, Stocklin G. Preparation of NCA 17-[^{18}F]fluoroheptadeconic acid in high yields via aminopolyether supported, nucleophilic fluorination. Journal of Labelled Compounds & Radiopharmaceuticals. 1986;23(5):455-66.

68. Adams DJ, Clark JH. Nucleophilic routes to selectively fluorinated aromatics. Chemical Society Reviews. 1999;28(4):225-31.

69. Dolci L, Dolle F, Jubeau S, Vaufrey F, Crouzel C. 2- [^{18}F]fluoropyridines by no-carrier-added nucleophilic aromatic substitution with [^{18}F]FK-K-222 - A comparative study. Journal of Labelled Compounds & Radiopharmaceuticals. 1999;42(10):975-85.

70. Rengan R, Chakraborty PK, Kilbourn MR. Can we predict reactivity for aromatic nucleophilic-substitution with [^{18}F]fluoride ion. Journal of Labelled Compounds & Radiopharmaceuticals. 1993;33(7):563-72.

71. Haskali MB, Telu S, Lee Y-S, Morse CL, Lu S, Pike VW. An Investigation of (Diacetoxyiodo)arenes as Precursors for Preparing No-Carrier-Added [^{18}F]Fluoroarenes from Cyclotron-Produced [^{18}F]Fluoride Ion. Journal of Organic Chemistry. 2016;81(1):297-302.

72. Lemaire C, Libert L, Plenevaux A, Aerts J, Franci X, Luxen A. Fast and reliable method for the preparation of ortho- and para- [^{18}F]fluorobenzyl halide derivatives: Key intermediates for the preparation of no-carrier-added PET aromatic radiopharmaceuticals. Journal of Fluorine Chemistry. 2012;138:48-55.

73. Tredwell M, Preshlock SM, Taylor NJ, Gruber S, Huiban M, Passchier J, et al. A General Copper-Mediated Nucleophilic [^{18}F]Fluorination of Arenes. Angewandte Chemie-International Edition. 2014;53(30):7751-5.

74. Flower DR. Modelling G-protein-coupled receptors for drug design. Biochimica Et Biophysica Acta-Reviews on Biomembranes. 1999;1422(3):207-34.

75. Trzaskowski B, Latek D, Yuan S, Ghoshdastider U, Debinski A, Filipek S. Action of Molecular Switches in GPCRs - Theoretical and Experimental Studies. Current Medicinal Chemistry. 2012;19(8):1090-109.

76. Kobilka BK, Deupi X. Conformational complexity of G-protein-coupled receptors. Trends in Pharmacological Sciences. 2007;28(8):397-406.

77. Rosenbaum DM, Rasmussen SGF, Kobilka BK. The structure and function of G-protein-coupled receptors. Nature. 2009;459(7245):356-63.

78. Kobilka BK. G protein coupled receptor structure and activation. Biochimica Et Biophysica Acta-Biomembranes. 2007;1768(4):794-807.

79. Stein RSL, Ehlert FJ. A kinetic model of GPCRs: analysis of G protein activity, occupancy, coupling and receptor-state affinity constants. Journal of Receptors and Signal Transduction. 2015;35(4):269-83.

80. Shalgunov V, van Waarde A, Booij J, Michel MC, Dierckx RAJO, Elsinga PH. Hunting for the high-affinity state of G-protein-coupled receptors with agonist tracers: Theoretical and practical considerations for positron emission tomography imaging. Medicinal research reviews. 2018.

81. Adham N, Gerald C, Schechter L, Vaysse P, Weinshank R, Branchek T. [^{3}H]5-Hydroxytryptamine labels the agonist high affinity state of the cloned rat 5-HT_4 receptor. European Journal of Pharmacology. 1996;304(1-3):231-5.

82. Brys R, Josson K, Castelli MP, Jurzak M, Lijnen P, Gommeren W, et al. Reconstitution of the human 5-HT_{1D} receptor-G-protein coupling: Evidence for constitutive activity and multiple receptor conformations. Molecular Pharmacology. 2000;57(6):1132-41.

83. Fillion G, Fillion MP. Transitional states of the neuronal serotonergic site. Eur J Pharmacol. 1980;65(1):109-12.

84. Seneca N, Finnema SJ, Farde L, Gulyas B, Wikstrom HV, Halldin C, et al. Effect of amphetamine on dopamine D2 receptor binding in nonhuman primate brain: A comparison of the agonist radioligand [^{11}C]MNPA and antagonist [^{11}C]raclopride. Synapse. 2006;59(5):260-9.

85. Clawges HM, Depree KM, Parker EM, Graber SG. Human 5-HT1 receptor subtypes exhibit distinct G protein coupling behaviors in membranes from Sf9 cells. Biochemistry. 1997;36(42):12930-8.

86. Lesch KP, Waider J. Serotonin in the Modulation of Neural Plasticity and Networks: Implications for Neurodevelopmental Disorders. Neuron. 2012;76(1):175-91.

87. Hannon J, Hoyer D. Molecular biology of 5-HT receptors. Behavioural Brain Research. 2008;195(1):198-213.

88. Berger M, Gray JA, Roth BL. The Expanded Biology of Serotonin. Annual Review of Medicine. 2009;60:355-66.

89. Hoyer D, Hannon JP, Martin GR. Molecular, pharmacological and functional diversity of 5-HT receptors. Pharmacology Biochemistry and Behavior. 2002;71(4):533-54.

90. Meyer JH, Wilson AA, Ginovart N, Goulding V, Hussey D, Hood K, et al. Occupancy of serotonin transporters by paroxetine and citalopram during treatment of depression: A [^{11}C]DASB PET imaging study. American Journal of Psychiatry. 2001;158(11):1843-9.

91. Fowler JS, Logan J, Volkow ND, Wang GJ, MacGregor RR, Ding YS. Monoamine oxidase: radiotracer development and human studies. Methods. 2002;27(3):263-77.

92. Best J, Nijhout HF, Reed M. Serotonin synthesis, release and reuptake in terminals: a mathematical model. Theoretical Biology and Medical Modelling. 2010;7.

93. Pineyro G, Blier P. Autoregulation of serotonin neurons: Role in antidepressant drug action. Pharmacological Reviews. 1999;51(3):533-91.

94. Kristensen AS, Andersen J, Jorgensen TN, Sorensen L, Eriksen J, Loland CJ, et al. SLC6 Neurotransmitter Transporters: Structure, Function, and Regulation. Pharmacological Reviews. 2011;63(3):585-640.

95. Cools R, Nakamura K, Daw ND. Serotonin and Dopamine: Unifying Affective, Activational, and Decision Functions. Neuropsychopharmacology. 2011;36(1):98-113.

96. Watanabe MAE, Nunes SOV, Amarante MK, Guembarovski RL, Oda JMM, De Lima KWA, et al. Genetic polymorphism of serotonin transporter 5-HTTLPR: involvement in smoking behaviour. Journal of Genetics. 2011;90(1):179-85.

97. Varnas K, Hall H, Bonaventure P, Sedvall G. Autoradiographic mapping of 5-HT_{1B} and 5-HT_{1D} receptors in the post mortem human brain using [^{3}H]GR 125743. Brain Research. 2001;915(1):47-57.

98. Hoyer D, Clarke DE, Fozard JR, Hartig PR, Martin GR, Mylecharane EJ, et al. International union of pharmacology classification of receptors for 5-Hydroxytryptamine (serotonin). Pharmacological Reviews. 1994;46(2):157-203.

99. Paterson LM, Kornum BR, Nutt DJ, Pike VW, Knudsen GM. 5-HT radioligands for human brain imaging with PET and SPECT. Medicinal Research Reviews. 2013;33(1):54-111.

100. Ruf BM, Bhagwagar Z. The 5-HT_{1B} Receptor: A Novel Target for the Pathophysiology of Depression. Current Drug Targets. 2009;10(11):1118-38.

101. Paterson LM, Tyacke RJ, Nutt DJ, Knudsen GM. Measuring endogenous 5-HT release by emission tomography: promises and pitfalls. Journal of Cerebral Blood Flow and Metabolism. 2010;30(10):1682-706.

102. Barnes NM, Sharp T. A review of central 5-HT receptors and their function. Neuropharmacology. 1999;38(8):1083-152.

103. Moret C, Briley M. The possible role of 5-$HT_{1B/D}$ receptors in psychiatric disorders and their potential as a target for therapy. European Journal of Pharmacology. 2000;404(1-2):1-12.

104. Sari Y. Serotonin(1B) receptors: from protein to physiological function and behavior. Neuroscience and Biobehavioral Reviews. 2004;28(6):565-82.

105. Yin WC, Zhou XE, Yang DH, de Waal PW, Wang MT, Dai AT, et al. Crystal structure of the human 5-HT_{1B} serotonin receptor bound to an inverse agonist. Cell Discovery. 2018;4.

106. Wang C, Jiang Y, Ma JM, Wu HX, Wacker D, Katritch V, et al. Structural Basis for Molecular Recognition at Serotonin Receptors. Science. 2013;340(6132):610-4.

107. Elling CE, Frimurer TM, Gerlach LO, Jorgensen R, Holst B, Schwartz TW. Metal ion site engineering indicates a global toggle switch model for seven-transmembrane receptor activation. Journal of Biological Chemistry. 2006;281(25):17337-46.

108. Pierson ME, Andersson J, Nyberg S, McCarthy DJ, Finnema SJ, Varnas K, et al. [^{11}C]AZ10419369: A selective 5-HT_{1B} receptor radioligand suitable for positron emission tomography (PET). Characterization in the primate brain. Neuroimage. 2008;41(3):1075-85.

109. Nabulsi N, Huang Y, Weinzimmer D, Ropchan J, Frost JJ, McCarthy T, et al. High-resolution imaging of brain 5-HT_{1B} receptors in the rhesus monkey using [^{11}C]P943. Nuclear Medicine and Biology. 2010;37(2):205-14.

110. Andersson JD, Pierson ME, Finnema SJ, Gulyas B, Heys R, Elmore CS, et al. Development of a PET radioligand for the central 5-HT_{1B} receptor: radiosynthesis and characterization in cynomolgus monkeys of eight radiolabeled compounds. Nuclear Medicine and Biology. 2011;38(2):261-72.

111. Cosgrove KP, Kloczynski T, Nabulsi N, Weinzimmer D, Lin SF, Staley JK, et al. Assessing the Sensitivity of [^{11}C]P943, a Novel 5-HT_{1B} Radioligand, to Endogenous Serotonin Release. Synapse. 2011;65(10):1113-7.

112. Finnema SJ, Varrone A, Hwang TJ, Gulyas B, Pierson ME, Halldin C, et al. Fenfluramine-Induced Serotonin Release Decreases [^{11}C]AZ10419369 Binding to 5-HT_{1B}-Receptors in the Primate Brain. Synapse. 2010;64(7):573-7.

113. Yang KC, Takano A, Halldin C, Farde L, Finnema SJ. Serotonin concentration enhancers at clinically relevant doses reduce [^{11}C]AZ10419369 binding to the 5-HT_{1B} receptors in the nonhuman primate brain. Translational Psychiatry. 2018;8.

114. Jorgensen LM, Weikop P, Svarer C, Feng L, Keller SH, Knudsen GM. Cerebral serotonin release correlates with [^{11}C]AZ10419369 PET measures of 5-HT_{1B} receptor binding in the pig brain. Journal of Cerebral Blood Flow and Metabolism. 2018;38(7):1243-52.

115. Deen M, Hansen HD, Hougaard A, da Cunha-Bang S, Norgaard M, Svarer C, et al. Low 5-HT_{1B} receptor binding in the migraine brain: A PET study. Cephalalgia. 2018;38(3):519-27.

116. Tiger M, Ruck C, Forsberg A, Varrone A, Lindefors N, Halldin C, et al. Reduced 5-HT_{1B} receptor binding in the dorsal brain stem after cognitive behavioural therapy of major depressive disorder. Psychiatry Research-Neuroimaging. 2014;223(2):164-70.

117. Varrone A, Svenningsson P, Forsberg A, Varnas K, Tiger M, Nakao R, et al. Positron emission tomography imaging of 5-hydroxytryptamine(1B) receptors in Parkinson's disease. Neurobiology of Aging. 2014;35(4):867-75.

118. Murrough JW, Henry S, Hu JA, Gallezot JD, Planeta-Wilson B, Neumaier JF, et al. Reduced ventral striatal/ventral pallidal serotonin(1B) receptor binding potential in major depressive disorder. Psychopharmacology. 2011;213(2-3):547-53.

119. Clark J, Baldwin R, Bayne K, Brown M, Gebhart G, Gonder J. Guide for the care and use of laboratory animals. National acadamey press; 2008.

120. Halldin C, Swahn CG, Farde L, Sedvall G. Radioligand disposition and metabolism: Key information in early drug development. Comar D, editor: Kluwer Academic Publishers; 1995.

121. Moein MM, Nakao R, Amini N, Abdel-Rehim M, Schou M, Halldin C. Sample preparation techniques for radiometabolite analysis of positron emission tomography radioligands; trends, progress, limitations and future prospects. Trac-Trends in Analytical Chemistry. 2019;110:1-7.

122. Lammertsma AA, Hume SP. Simplified reference tissue model for PET receptor studies. Neuroimage. 1996;4(3 Pt 1):153-8.

123. Varnas K, Hall H, Bonaventure P, Sedvall G. Autoradiographic mapping of 5-HT_{1B} and 5-HT_{1D} receptors in the post mortem human brain using [^{3}H]GR 125743. Brain Res. 2001;915(1):47-57.

124. Frisch MJ, Trucks GW, Schlegel HB, Scuseria GE, Robb MA, Cheeseman JR, et al. Gaussian 09 Revision. A. 2nd ed. Wallingford CT: Gaussian Inc; 2009.

125. Lindberg A, Nag S, Schou M, Takano A, Matsumoto J, Amini N, et al. [^{11}C]AZ10419096 - a full antagonist PET radioligand for imaging brain 5-HT_{1B} receptors. Nucl Med Biol. 2017;54:34-40.

126. Liow J-S, Lu S, Zoghbi SS, Gladding RL, Morse C, Hirvonen J, et al. C-11 CUMI-101, an agonist radioligand for serotonin 5-HT_{1A} receptors, also binds to brain alpha(1)-adrenoceptors in rodents and monkeys. Neuroimage. 2010;52:S56-S7.

127. Peng T, Zysk J, Dorff P, Elmore CS, Strom P, Malmquist J, et al. D2 Receptor Occupancy in Conscious Rat Brain is Not Significantly Distinguished With [^{3}H]MNPA, [^{3}H](+)-PHNO, and [^{3}H]Raclopride. Synapse. 2010;64(8):624-33.

128. McCormick PN, Kapur S, Seeman P, Wilson AA. Dopamine D2 receptor radiotracers [^{11}C](+)-PHNO and [^{3}H]raclopride are indistinguishably inhibited by D2 agonists and antagonists ex vivo. Nuclear Medicine and Biology. 2008;35(1):11-7.

129. Taylor NJ, Emer E, Preshlock S, Schedler M, Tredwell M, Verhoog S, et al. Derisking the Cu-Mediated ^{18}F-Fluorination of Heterocyclic Positron Emission Tomography Radioligands. Journal of the American Chemical Society. 2017;139(24):8267-76.

130. Zhou FC, Tao-Cheng JH, Segu L, Patel T, Wang Y. Serotonin transporters are located on the axons beyond the synaptic junctions: Anatomical and functional evidence. Brain Research. 1998;805(1-2):241-54.